PNNL-11310
UC-2030

RECEIVED
SEP 30 1996
OSTI

Gas Release During Salt Well Pumping: Model Predictions and Comparisons to Laboratory Experiments

L. M. Peurrung
S. M. Caley
E. Y. Bian
P. A. Gauglitz

September 1996

Prepared for the U.S. Department of Energy
under Contract DE-AC06-76RLO 1830

Pacific Northwest National Laboratory
Operated for the U.S. Department of Energy
by Battelle

Battelle

PNNL-11310

DISTRIBUTION OF THIS DOCUMENT IS UNLIMITED

MASTER

DISCLAIMER

This report was prepared as an account of work sponsored by an agency of the United States Government. Neither the United States Government nor any agency thereof, nor Battelle Memorial Institute, nor any of their employees, makes any warranty, express or implied, or assumes any legal liability or responsibility for the accuracy, completeness, or usefulness of any information, apparatus, product, or process disclosed, or represents that its use would not infringe privately owned rights. Reference herein to any specific commercial product, process, or service by trade name, trademark, manufacturer, or otherwise does not necessarily constitute or imply its endorsement, recommendation, or favoring by the United States Government or any agency thereof, or Battelle Memorial Institute. The views and opinions of authors expressed herein do not necessarily state or reflect those of the United States Government or any agency thereof.

PACIFIC NORTHWEST NATIONAL LABORATORY
operated by
BATTELLE
for the
UNITED STATES DEPARTMENT OF ENERGY
under Contract DE-AC06-76RLO 1830

Printed in the United States of America

Available to DOE and DOE contractors from the Office of Scientific and Technical Information, P.O. Box 62, Oak Ridge, TN 37831; prices available from (615) 576-8401.

Available to the public from the National Technical Information Service, U.S. Department of Commerce, 5285 Port Royal Rd., Springfield, VA 22161

The document was printed on recycled paper.

PNNL-11310
UC-2030

Gas Release During Salt Well Pumping: Model Predictions and Comparisons to Laboratory Experiments

L. M. Peurrung
S. M. Caley
E. Y. Bian
P. A. Gauglitz

September 1996

Prepared for
the U.S. Department of Energy
under Contract DE-AC06-76RLO 1830

Pacific Northwest National Laboratory
Richland, Washington 99352

DISCLAIMER

Portions of this document may be illegible in electronic image products. Images are produced from the best available original document.

Executive Summary

The Hanford Site has 149 single-shell tanks (SSTs) containing radioactive wastes that are complex mixes of radioactive and chemical products. Some of these wastes are known to generate mixtures of flammable gases, including hydrogen, nitrous oxide, and ammonia. Nineteen of these SSTs have been placed on the Flammable Gas Watch List (FGWL) because they are known or suspected, in all but one case, to retain these flammable gases. Salt well pumping to remove the interstitial liquid from SSTs is expected to cause the release of much of the retained gas, posing a number of safety concerns. Research at the Pacific Northwest National Laboratory (PNNL)[(a)] has sought to quantify the release of flammable gases during salt well pumping operations. This study is being conducted for Westinghouse Hanford Company as part of the PNNL Flammable Gas Project. Understanding and quantifying the physical mechanisms and waste properties that govern gas release during salt well pumping will help to resolve the associated safety issues.

There has been little previous work on the how salt well pumping releases trapped gas. Still, it is expected that gas trapped in salt cake waste will be released during salt well pumping, but only simple models predicting the gas release behavior are available.

The objective of this study was to use a computer model, STOMP, simulating multiphase flow in porous media to predict the release rate and cumulative release of flammable gases from SSTs as a result of salt well pumping. This model sought to include the salt well pumping operational parameters and the physical properties of the SST wastes that will affect the release of flammable gases. To validate the model for operations of this type, laboratory experiments were performed to measure insoluble gas release as a result of draining liquid from permeable media. Agreement between the laboratory data and model predictions was good, establishing the applicability of the model for insoluble gases. Validity for studying soluble gases such as ammonia should be explored in future work.

Simulations have been completed for a simple, one-dimensional model that demonstrates many of the physical processes and a two-dimensional model that reflects actual tank geometry. The results of the one-dimensional simulations suggest that, as the retreating liquid exposes the trapped gas bubbles, the trapped gas is released by diffusing through the connected gas channels to the surface of the salt cake. As expected, essentially all of the gas in the exposed bubbles is released, although the release rate depends on a number of parameters. Second, as the liquid head is reduced during the draining process, the trapped gas bubbles expand. Depending on the parameter range, these expanded bubbles may connect and allow gas flow or may remain trapped until exposed to the invading gas by the retreating liquid.

(a) Pacific Northwest National Laboratory is operated for the U.S. Department of Energy by Battelle under Contract DE-AC06-76RLO 1830.

One of the most interesting results demonstrated by the one-dimensional simulations is the effect of the liquid draining rate (equivalent to salt well pumping rate) on the gas release rate. When the draining rate is slow, on the order of 100 days, the gas diffuses upwind against the invading gas once the bubbles are exposed. In this situation, the diffusion rate is faster than the flow rate of the invading gas, and the release rate of gas is proportional to the draining rate; this confirms existing simple models. A small increase in the release rate occurs when pumping ceases, because in the absence of inward flow of air, the gas in exposed bubbles releases more effectively by diffusion.

When the draining rate is fast, about one day, the diffusion rate of gas from exposed bubbles is slower than the rate of invading gas. In this situation, there is negligible diffusion upwind against the invading gas and thus no release during draining. However, when the liquid draining ceases, the previously trapped gas is easily released by diffusion, giving a larger-than-expected release rate. In actual salt well pumping, the waste is drained over hundreds of days; therefore, the gas release behavior will be like that described for the slow draining rate results.

Simulation results for a two-dimensional configuration typical of SSTs show behavior similar to one-dimensional results. For these simulations, the release of both an insoluble gas (to represent hydrogen) and a soluble gas (to represent ammonia) were modeled. Approximately half the liquid drained from the salt cake in two-dimensional simulations, while half remained trapped in the interstitial pores by capillary forces; the liquid pumping rate was initially limited to 19 L (5 gal)/min and fell to about 2 L (0.5 gal)/min after 50 days of continuous pumping.

Draining the pumpable liquid released virtually all of the undissolved gas in the bubbles. Penetration of the salt cake by invading air exposed the bubbles, allowing their gases to diffuse to the surface of the salt cake during draining. A total of 56.6 m^3 (2000 SCF) of the insoluble gas was released over 60 to 100 days. The highest instantaneous release rate was approximately 0.003 m^3/min (0.10 scfm), or 4.3 m^3 (150 ft^3)/day. At a ventilation rate of 0.14 m^3/min (5 scfm) or 200 m^3 (7200 ft^3)/day, this release could potentially cause the hydrogen concentration to exceed 25% of the lower flammability limit. However, more detailed dome space calculations would be necessary to support this conclusion.

The soluble gas release rate was found to be greatly accelerated by salt well pumping. Draining the liquid from the salt cake created a large gas/liquid interfacial area, which, in turn, increased the mass transfer and release rates of the soluble gas. STOMP showed releases of up to 11,327 m^3 (400,000 SCF) of soluble gas over 500 days and instantaneous release rates as high as 181 m^3 (6400 ft^3)/day. However, these results seem high compared with operational experience and are based on several assumptions, including a very large ventilation rate. A limited ventilation rate would simply result in a dome space saturated with vapor and a lower vapor release rate. Mass transfer limitations in the liquid phase and salt cake slumping could also reduce release rates. In practice, salt well pumping may simply accelerate the release of ammonia to the dome space.

Finally, the two-dimensional simulations showed that little undissolved gas (less than 0.425 m^3 [15 SCF]) is released into the well during pumping.

Acknowledgments

The authors wish to thank Mark D. White of PNNL for his important contributions to this work. Mark, who is the primary developer of the STOMP code, made a number of modifications that allowed STOMP to model gas release during salt well pumping, checked the code results for consistency in this application, helped resolve a number of numerical difficulties and generally provided valuable expert counsel.

Contents

Figures

Tables

1.0 Introduction

The Hanford Site has 149 single-shell tanks (SSTs) containing radioactive wastes that are complex mixes of radioactive and chemical products. Some of these wastes are known to generate mixtures of flammable gases, including hydrogen, nitrous oxide, and ammonia. Nineteen of these SSTs have been placed on the Flammable Gas Watch List (FGWL) because they are known or suspected, in all but one case, to retain these flammable gases (Hopkins 1995; Hanlon 1995). Salt well pumping to remove the interstitial liquid from SSTs is expected to cause the release of much of the retained gas, posing a number of safety concerns. Research at the Pacific Northwest National Laboratory (PNNL)[a] has sought to quantify the release of flammable gases during salt well pumping operations. This study is being conducted for Westinghouse Hanford Company as part of the PNNL Flammable Gas Project. Understanding and quantifying the physical mechanisms and waste properties that govern gas release during salt well pumping will help to resolve the associated safety issues.

Salt well pumping, or interim stabilization, is a well-established operation that began in the mid-1970s for removing drainable interstitial liquid from SSTs (Grimes 1978). While salt well pumping has been conducted in many tanks for years, there has been little previous work on how it releases retained gas. In general, understanding gas release mechanisms in SSTs is in an early stage of development, but preliminary studies are beginning to elucidate the most likely behavior.[b] Still, there is evidence that certain SSTs are retaining gas in amounts that, if released rapidly compared with the mixing and dilution within the dome space of the tanks, could lead to a flammable condition in the tank dome space (Hodgson et al. 1995, 1996; Whitney 1995).

Salt well pumping of SSTs on the FGWL is expected to begin soon, so it is necessary to understand the release rate and cumulative release of flammable gases. Currently, Los Alamos National Laboratory (LANL) is preparing a safety assessment for salt well pumping FGWL tanks; this work represents the most thorough discussion of how gas releases might occur as a result of salt well pumping.[c] As part of this safety assessment, Spore[d] estimated the release rate of gas initially

---

(a) Pacific Northwest National Laboratory is operated for the U.S. Department of Energy by Battelle under Contract DE-AC06-76RLO 1830.

(b) A variety of plausible gas release mechanisms were discussed by RT Allemann et al. in a letter report entitled, *A Discussion of Some Release Mechanisms for Sudden Gas Release from Single-Shell Tanks at Hanford* (PNL-WTS-101095) (October 1995).

(c) This safety assessment is currently the draft document WHC-SD-WM-SAD-034 Rev. 0, *A Safety Assessment for Salt Well Jet Pumping Operations in Tank 241-A-101: Hanford Site, Richland, Washington* (1996).

(d) Spore, JW. 1996. *Conservative Gas Releases for Tank 241-A-101.* Los Alamos National Laboratory Calc-Note, TSA10-CN-WT-SA-GR-046.

trapped in bubbles as a result of draining liquid from a SST (the model neglected the release of soluble gases such as ammonia). In this model, it was assumed that, as the waste was drained, all of the trapped gas bubbles in the drained region were released. The consequence of this assumption is that the release rate was proportional to the salt well pumping rate.

Single-shell tank waste has a range of physical properties and is typically classified as sludge, salt cake, or supernatant liquid (Hanlon 1995). Hanlon (1995) describes salt cake as waste that resulted from crystallization and precipitation after concentration of liquid waste and that is composed of precipitated salt crystals. Generally, salt cake waste has a noticeable particulate character that varies from gravel-sized chunks to fine particles, but generally the particles are larger than the colloidal size of about 1 micron. Sludges are wet solids (insoluble) that were formed (precipitated) during sodium hydroxide additions to the waste. Unlike salt cake, sludges typically have very small particle sizes, below 1 micron, and are described as clay-like and plastic materials.

Flammable gases are retained in tank waste as both gas bubbles and dissolved gas (primarily ammonia). The principal mechanisms of bubble retention and details of specific bubble retention mechanisms have been discussed previously (Gauglitz et al. 1994, 1995, 1996; Rassat and Gauglitz 1995). Observations of bubble retention in both actual SST and double-shell tank (DST) waste have also been reported (Gauglitz et al. 1996; Bredt et al. 1995; Bredt and Tingey 1996). For bubbles retained in particulate simulated waste (salt cake with coarse particles), the previous work showed that the morphology of the retained bubbles depends on a Bond number, which is a ratio of gravitational forces to surface tension. Where the waste has relatively coarse particles typical of salt cake (on the order of 10 to 100 microns), it is expected that the dominant bubble retention mechanism will be capillary force and that the bubbles will finger between the particles constituting the particulate medium.

Many of the SSTs, those containing primarily sludge and those containing primarily salt cake, are expected to be salt well pumped. Only the tanks containing permeable salt cake are expected to show substantial removal of liquid, and we believe these are more likely to release flammable gases. Accordingly, our purposes are to understand the physical phenomena that occur during salt well pumping of salt cake-type waste and to determine how these phenomena govern the release of gas.

1.1 Objectives

The specific focus of this study is predicting release rates and cumulative release of flammable gases from SSTs as a result of salt well pumping, using a computer model of multiphase flow in porous media. The first objective was to modify an existing computer model for simulating fluid transport in porous media (STOMP) to model the release of trapped gas as a result of salt well pumping. In this model, we seek to include the salt well pumping operational parameters and the physical properties of the SST wastes that will affect the release of flammable gases. The modifications to the STOMP code were tested by simulating liquid draining and gas release from a one-dimensional column. The validity of those results was evaluated by performing laboratory experiments with columns, comparing model predictions with measured gas release. The one-dimensional simulations were also used to learn about the physical phenomena occurring during salt well pumping. The second objective was to apply the model to a two-dimensional geometry

reflecting the actual geometry of an SST and predict the gas release rate during salt well pumping. In the study of the actual tank geometry, both insoluble (representing hydrogen) and soluble (representing ammonia) gases were considered. Together, these modeling results help to quantify the physical phenomena occurring during salt well pumping and estimate the gas release rate in a typical tank.

1.2 Salt Well Pumping of Salt Cake SSTs

Figure 1.1 depicts salt well pumping in an SST containing salt cake. Interstitial liquid drains through the screened interval of the salt well, where it is removed by a pump. In the vicinity of the salt well screen, the fluid level is reduced most quickly, while the fluid level away from the well decreases more slowly. Draining the fluid draws air into the pores between the salt crystals. Once the air has invaded the pores and exposed previously trapped bubbles, the gas within these bubbles can be released from the waste. Also shown in the figure is the expansion of bubbles caused by the reduced hydrostatic head on the bubbles as the liquid is drained from the waste. When the gas void fraction is low, these bubbles will simply expand. In contrast, if the gas fraction is sufficiently high, the expanding bubbles will connect and flow upward. In general, the gas fraction that defines the transition where bubbles connect depends on the porosity and connectedness of the pores and the distribution of the retained bubbles. While this transition depends on many things that are difficult to measure, it is an easy parameter to vary in models.

Porosity designates the volume fraction of the porous medium not occupied by the solid phase. The terms gas saturation and either gas fraction or void fraction refer to the volume fraction of gas, but not interchangeably. Gas saturation is used to refer to the portion of the porosity occupied by a gas phase. Gas saturation therefore ranges from 0 (fully liquid-saturated salt cake) to 1 (dry salt cake). Gas fraction or void fraction is the part of the total volume occupied by gas, ranging from zero up to the value of the porosity. Hence, void fraction equals gas saturation times porosity. While STOMP reports results in terms of gas saturation, tank waste studies typically refer to void fraction. When discussing results, this report will refer to both terms (e.g., "The final gas saturation was 0.65 [void fraction 0.26]") or will include a multiplier ("To convert to void fraction, multiply by 0.4.").

The hydraulic properties of salt cake are expected to affect both salt well pumping and gas release behavior. However, only a few studies are available for estimating the hydraulic properties of SST waste. Metz (1976) estimated a 19 Darcy permeability for salt cake in Tank 241-BY-107. While this is probably the only estimate available for actual tank waste, it is likely that more recent salt well pumping data could be analyzed following Metz's approach or one similar. Strachan (1975a, 1975b) measured the permeability of synthetic salt cake and found it to be about 2 darcies. Handy (1975), however, measured a 22-darcy permeability for a synthetic salt cake. While there is some range in these permeability estimates, they are typical of a porous medium of 100-micron

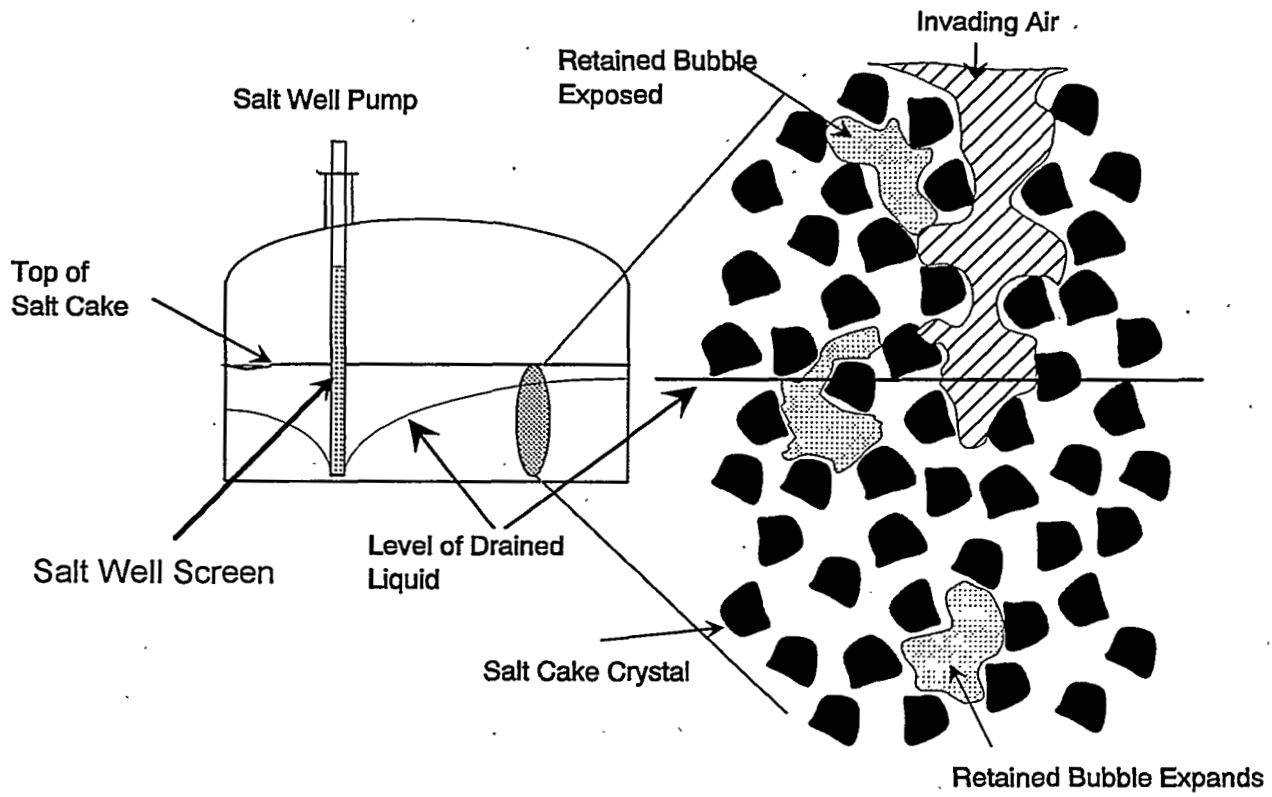

Figure 1.1. Draining Interstitial Liquid, Causing Invading Air to Expose Retained Bubbles and Retained Bubbles to Expand as the Fluid Head Decreases

particles.[a] Based on these studies, we believe that it is reasonable to assume that the salt cake waste will behave as a somewhat typical porous medium as we seek to understand how gases and fluids behave in a salt cake SST (Simmons 1996).[b]

(a) In a recent letter report, RJ Lenhard (PNNL) used the permeability estimates from Metz (1975) to estimate the pore size (about 30 micron diameter) of the salt cake in Tank 241-BY-107. *Assessment of Average Salt-Cake Pore Sizes in Tank 241-BY-107 at Hanford and Determination of a Particle-Size Distribution for a Salt Cake Surrogate*, January 20, 1995.

(b) CS Simmons has reviewed the liquid retention behavior of tank waste and believes that it is reasonable to treat it as a permeable medium. This work is also contained in a 1995 draft report, *A Simplified Model of Salt Cake Moisture Distribution.*

To understand how gas is released during salt well pumping, it is important to have reasonable estimates for the volume of trapped gas in the waste. While a large amount of information is available on the FGWL tanks (see Brager 1994, for example), there is essentially no direct information on the quantity or fraction of gas retained in SSTs. In comparison, in situ measurements of void fraction have been collected for six DSTs (Stewart et al. 1996, 1995; Shepard et al. 1995).[a] Although direct data do not exist on the void fraction in SSTs, a number of studies have made estimates of retained gas volumes. Whitney (1995) has screened Hanford tanks for trapped gas by correlating the changes in waste level with barometric pressure fluctuations due to gas bubbles compressing and expanding. Hopkins (1995) has presented a methodology for evaluating trapped gas in Hanford waste tanks that includes both the barometric pressure evaluation and level increases in the waste. Hodgson et al. (1995, 1996) presented an evaluation of a number of tanks based on the methodology described by Hopkins (1995).

The evaluation by Hodgson et al. (1995, 1996) focused on determining the largest potential flammable gas concentration in the dome space of the tanks. While retained void fractions are not directly reported in the evaluation, the results can be used to directly calculate the void fraction in the settled solids layer in the tanks. It should be emphasized that the method of Hopkins (1995) and the evaluation of Hodgson et al. (1995, 1996) used data and tank parameters that had a large uncertainty associated with them. Still, the estimates of void fraction are useful.

Table 1.1 shows the estimated percent of gas-occupied voids in the tanks on the FGWL. These estimates are based on the barometric pressure evaluation (50th percentile) using the data in the appendixes of Hodgson et al. (1996) and the methodology presented by Hopkins (1995). The barometric pressure estimates represent best estimates and are reasonable estimates of the actual gas fraction in the tank waste (we have only included those estimates based on FIC or Enraf level data). For example, an average in situ void fraction of 0.069 (percent void of 6.9) was measured with the void fraction instrument in SY-103 (Shepard et al. 1995), and Table 1.1 gives an estimate of 0.05. The void fraction results in Table 1.1 show that a number of tanks, both SSTs and DSTs, retain a substantial void fraction.

(a) Void fraction results for three of these six tanks have also been reported in letter reports by C. Stewart, JM Alzheimer, CL Shepard, G Terrones, G Chen, and NE Wilkins entitled, *In Situ Determination of Rheological Properties and Void Fraction: Hanford Waste Tank 241-AW-101* (PNL-MIT-110195, October 1995); *In Situ Determination of Rheological Properties and Void Fraction: Hanford Waste Tank 241-AN-105* (PNL-MIT-021696, February 1996); and *In Situ Determination of Rheological properties and Void Fraction: Hanford Waste Tank 241-AN-104* (TWSMIT:060796, June 1996).

Table 1.1. Void Fraction Estimates for Flammable Gas Watch List Tanks[a]

Tank	Void Fraction (%) Based on 50th percentile Barometric Pressure Evaluation Results
Single-Shell Tanks	
A-101	
AX-101	
AX-103	
S-102	19
S-111	14
S-112	
SX-101	
SX-102	13
SX-103	18
SX-104	
SX-105	
SX-106	9
SX-109	
T-110	
U-103	11
U-105	10
U-107	8
U-108	
U-109	8
Double-Shell Tanks	
AN-103	20
AN-104	8
AN-105	8
AW-101	7
SY-101	10
SY-103	5

(a) Hopkins (1995) presented a methodology for evaluating trapped gas in Hanford waste tanks, and Hodgson et al. (1995, 1996) presented an evaluation of a number of tanks based on this methodology. The 50th percentile barometric pressure estimates were obtained from the data reported in Hodgson et al. (1996), and we include here only those void fractions based on FIC or Enraf dL/dP results.

2.0 Modeling Approach

STOMP (Subsurface Transport Over Multiple Phases) is a simulator for analyzing flow and transport through porous media. It has been developed at PNNL and used primarily for modeling soil hydrology. STOMP is coded in FORTRAN 77 and solves differential equations representing mass balances on air, water, and other phases (e.g., oil or ice) using the integral volume finite difference technique. Flows are Darcy-type based on the intrinsic and relative permeability of the porous medium and its liquid and gas phases. Simulation geometry, physical properties, and initial and boundary conditions are entered via an input file. The simulator's outputs are time- and position-dependent pressures, fluid saturations, concentrations, and fluxes. STOMP can also calculate an energy balance to solve nonisothermal problems, but this capability was not used for this study. This section of the report describes the physics included in the model and how it was applied to salt well pumping. For further details on the mathematics and solution technique, see the STOMP manuals.[a]

STOMP models gas and liquid flow through an immobile, porous, solid phase. It is therefore well suited for studying salt well pumping.[b] However, salt cake "slumping" or subsidence will not be considered in the results described in this report, nor will yielding of material. As discussed in Section 1, the validity of applying this model to tank waste depends on the degree to which salt cake behaves like a typical permeable material. However, we believe that description is appropriate.

2.1 Modeling the Gas Phase

Because STOMP is a finite difference model, the solution domain is discretized on a grid to form "elements" or "nodes." For example, to simulate draining a tank in the vertical dimension only, a 9-m (30-ft)-high column of waste might be discretized into 30, 30.5-cm (1-ft)-tall elements. Each element is assumed to be homogeneous; that is, physical properties, saturations, concentrations, and pressures are assumed to be uniform within the element. Thus, there are no details of phenomena occurring on length scales shorter than an element width. Instead, microscopic behavior is accounted for by the governing equations on macroscopic variables, which is a well-established method of modeling multiple phases in porous media (Dullien 1992).

For this reason, STOMP does not model individual bubbles, which are too small to be resolved by discretization. Instead, each element has a homogeneous gas phase volume fraction. The bubble-like behavior of the gas is incorporated through the constitutive equations used to relate gas and liquid phase pressures to gas saturation. The constitutive model used for this report is a relation based on the work of Parker and Lenhard (1987a, 1987b) that allows gas to be trapped during

---

(a) White, M,D and M Oostrom. 1995. *STOMP User's Guide* (draft) and *STOMP Theory Guide* (draft). WE Nichols et al. 1995. *STOMP Application Guide* (draft). Pacific Northwest National Laboratory, Richland, Washington.

(b) CS Simmons has been using STOMP to model liquid retention behavior of tank waste in another Tank Waste Safety project.

imbibition. By using this form, a static initial condition is possible with a certain volume fraction of gas immobilized or "trapped" in the otherwise saturated salt cake. The model also allows the element to contain, simultaneously, some gas that is not trapped and is connected to gas spaces in adjacent elements. While there are no "round" or "dendritic" bubbles in STOMP (since they are too small to be resolved), the flavor of the model is of dendritic bubbles of two length scales:

1) smaller than the width of the element and participate in intra-element transport only

2) span the width of the element and participate in inter- and intra-element transport.

In the model, there is a limit to the amount of gas that can be kept in a trapped state, above which the trapped gas begins to coalesce and become interconnected. This "maximum trapped gas saturation" is set by the user at a fixed, global value that applies to the whole porous medium. However, the *local* maximum trapped gas fraction at a point may be less than the *global* value due to that point's drainage/imbibition history. That is, if the element has been only partially drained and reimbibed, some of the locations where trapped gas could be held are assumed to be lost.

To illustrate the nature of the trapped and free gas, consider the gas fraction in a submerged element as the liquid level slowly falls. Initially, only trapped gas is present – in this example, a 5% gas saturation out of a 10% maximum before coalescence and flow occurs. There are no gas fluxes since all gas is fixed in place and does not contribute to transport between elements. As liquid drains and the liquid level falls, gas saturation increases due to the decrease in pressure. If the absolute pressure were to fall by a factor of two, the trapped gas would swell until it exceeded the maximum saturation. The fraction in excess of 10% would then become free gas, interlinked with the free gas above it, and would flow upwards. (Potentially, the flow could decrease the gas saturation until it fell below the maximum, resulting in pulses of gas up through the medium. This bubble-like gas release was what we originally expected the model to show. In STOMP, however, the gas release tends to be more steady. Gas fluxes out of these bubbles are kept small because the gas relative permeability is strongly dependent on the free gas saturation. As the free gas saturation increases, the relative permeability increases just enough to release gas at an equal rate.)

As downward flow of liquid brings the liquid level down to a new element, the gas saturation in that element rises sharply as air begins to flow into it from above. In addition to this new free gas, the trapped gas is gradually freed. When the liquid level falls past the element to the one below it, opening it to gas flow, air begins to flow down through the element. Some of the air influx contributes to desaturating the element itself, while the rest flows through and desaturates lower elements.

If the liquid draining stopped, some of the trapped gas remaining in elements in the capillary fringe would remain trapped. Re-imbibing the elements would trap gas again (now composed of air as well as ammonia, hydrogen, etc.), but not necessarily the maximum amount.

2.2 Modeling the Bubble Gases as Solutes

STOMP includes solutes that can partition into the gas, liquid, or solid phases. STOMP also calculates the amount of air dissolved in the liquid phase and water vapor in the gas phase. In STOMP, all components within an element are at thermodynamic equilibrium, so there are no kinetics of evaporation or partitioning. Solutes are assumed to be passive tracers. They do not affect the physical properties of the gas or liquid phases, and they do not occupy any volume. Solutes instantaneously partition between gas and liquid phases according to a partition coefficient that relates their gas and liquid phase concentrations. Hence, the gas phase in an element is always saturated with the solute in the sense that the concentration in the gas is in equilibrium with that currently in the liquid. Note that this assumption would be in error if there were significant mass transfer limitations due to slow diffusion in the liquid. In general, however, the intimate contact between gas and liquid phases in porous media is such that this assumption is valid.

STOMP handles solute transport by first solving mass and energy balances on the gas and liquid phases, then calculating the resulting convective and diffusive fluxes of solutes in those phases. (Note that solutes in trapped gas phases do not participate in either type of flux.)

In this study, the gas bubbles released during salt well pumping were modeled as air bubbles containing passive tracer gases. STOMP cannot yet model other concentrated gases that are miscible in air and with each other. The drawback to this approach is that when a water-soluble gas such as ammonia partitions into the gas phase, there is no resulting change in gas volume. The model will therefore underpredict the gas saturation in elements with trapped gas, underpredicting instantaneous release rates of both insoluble and soluble gases. The total amount of soluble gas released when the tank is completely drained will also tend to be underpredicted, but not the total amount of insoluble gas. This effect is more important when the gas content of the tank is near the percolation threshold. The effect becomes negligible if the relative amount of insoluble gas present is high compared with the soluble gas. This issue is discussed further in Appendix A, where its effect on the model's gas release predictions is estimated.

Underpredicting gas release rates is a serious concern. We hope to add this capability to the model in the future.

2.3 Modeling the Tanks

Modeling the tanks requires specification of geometry, discretization scheme, pumping duration, physical properties and constitutive relations, and initial and boundary conditions. Typically the modeled waste is a cylinder 610–914 cm (20–30 ft) high with azimuthal symmetry, discretized into 40 to 160 elements vertically. For the one-dimensional modeling results, no radial variations were included. For the two-dimensional results, the domain has a diameter of 23 m (75 ft) with 10 radial elements. Simulations vary from 10 to 200 days of (simulated) time, including pumping time and time for released gas to dissipate from the salt cake.

For simplicity, the physical properties for the one-dimensional model results were chosen to approximate the behavior of water and one insoluble solute gas in a salt cake with the permeability of a poorly graded sand, similar to the permeability reported by Metz (1976). However, for the two-dimensional results, the fluid viscosity and density were raised to 24 cP and 1.4 g/cm^3, respectively, to simulate Tank A-101 liquid waste. Two solute gases were included, one with the gas-phase diffusivity and aqueous solubility of ammonia and an insoluble one with the diffusivity of hydrogen. The partition coefficient for the soluble gas was specified to be 5×10^{-3} (moles of solute/m^3 of gas)/(moles of solute/m^3 of aqueous phase). This partition coefficient corresponds to a Henry's Law constant of six moles of ammonia/kg water/atm ammonia measured for simulants (Norton and Pederson 1994). Other values of physical properties and their sources are listed in Table 2.1. A sample input file is included as Appendix B.

The initial condition for all simulations was static with the liquid level at the top of the salt cake. Trapped gas was distributed uniformly throughout the waste; gas and aqueous pressures were equilibrated at all positions.

No flux boundary conditions were imposed on the sides of the tank. Gas phase and solute phase fluxes were permitted through the top surface, but no gas flux was allowed through the bottom surface. A constant gas phase pressure was specified on the top surface. Accumulation of solute gas in the space above the upper surface was neglected, so a zero solute gas concentration was imposed there. For the 1-D model, a Neumann condition of constant liquid flux was imposed on the bottom surface.

Table 2.1. Typical Values of Physical Parameters Used in the STOMP Simulations[a]

Parameter	Typical Values		Units	Source/Basis
	1-D Model	2-D Model		
Porosity of solid phase	0.4		unitless	Typical of porous solids without large heterogeneities
Hydraulic conductivity	12	22	Darcy	Handy 1975, Metz 1976
van Genuchten alpha parameter	drainage: 5 imbibition: 10		1/m	Corresponds to a poorly graded sand
van Genuchten n parameter	1.25		unitless	Corresponds to a poorly graded sand
Residual liquid saturation	0.01		unitless	Typical of soils
Maximum entrapped air saturation (void fraction)	0.10 (0.04)	0.08 (0.032)	unitless	Somewhat arbitrary; depends on waste and gas configuration; chosen to exceed tank waste retained gas saturation
Gas phase diffusivity	tracer: 0.1	insoluble: 0.75; soluble: 0.25	cm^2/s	Welty et al. (1984) to mimic hydrogen, ammonia
Gas concentration	tracer: 1	insoluble: 23 soluble: 11	mol/m^3	30% / 15% at average pressure of 1.7 atm
Liquid phase diffusivity	$1.x10^{-5}$		cm^2/s	Typical of aqueous diffusion
Gas-aqueous partition coefficient	tracer: 10^{10}	insoluble: 10^{10}; soluble: 5×10^{-3}	m^3 aq/ m^3 gas	Tracer treated as essentially insoluble; soluble value based on Norton and Pederson (1994) for ammonia in tank waste
Initial trapped gas saturation (void fraction)	0.04-0.095 (0.016-0.038)	0.075 (0.30)	unitless	0.075 based on Kubic (1995), assumed porosity of 0.4
Air density	1.20		kg/m^3	Welty et al. (1984); assumption of T = 25°C
Liquid density	999.3	1400	kg/m^3	Handy (1975)
Liquid viscosity	1	24	cP	24 cP based on draft SA[b]

(a) For input parameter definitions, see *STOMP User's Guide* (draft), Pacific Northwest National Laboratory.
(b) WHC-SD-WM-SAD-034 Rev. 0, *A Safety Assessment for Salt Well Jet Pumping Operations in Tank 241-A-101: Hanford Site, Richland, Washington* (1996) (draft). This viscosity value is cited in Appendix G as a conservative one.

3.0 Results

The modeling results are divided into two sections. In the first section, the model was used to calculate a one-dimensional (1-D) solution to the general problem of draining a column of saturated porous material. The material properties were those of air and water with an essentially insoluble tracer gas. In the second, the full two-dimensional (2-D) solution was applied to simulate salt well pumping, using physical properties more like those of tank waste, hydrogen, and ammonia. The focus of the 1-D results is on showing a typical solution, illustrating some of the key physical phenomena, showing and discussing qualitative results, showing trends, and evaluating parametric sensitivity. The 1-D model results will also reveal some numerical artifacts of the solution method. Simplifying assumptions of air, water, and tracer were used to make the results easy to understand and interpret. For predicting gas releases during salt well pumping, however, the 2-D model is employed, with as many estimates of the properties of the waste as are available.

3.1 One-Dimensional Model Results

The results of the 1-D simulations suggest a number of important conclusions. First, as the retreating liquid exposes the trapped gas bubbles to invading air, the trapped gas is released by diffusing through the connected gas channels to the surface of the salt cake. As expected, essentially all of the gas in the exposed bubbles is released, although the release rate depends on a number of parameters. Second, as the liquid head is reduced during the draining process, the trapped gas bubbles expand. Depending on the parameter range, these expanded bubbles may connect and allow gas flow or remain trapped until exposed by the invading gas.

There are several artificial aspects of modeling salt well pumping in only one dimension. There are no radial fluxes, nor are there any radial variations in physical properties or variables. The fluid is not drawn out through a central well (such a well would have a radial extent); rather, the liquid is withdrawn uniformly across the bottom surface. However, we can use the 1-D model to infer many important, qualitative conclusions about the effect of salt well pumping on trapped gas.

3.1.1 Case Study 1: A Baseline

To illustrate a typical solution, consider a simple 100-day draw-down with an initial trapped gas saturation of 0.05 (void fraction = 0.02). Parameters used for this case are shown in Table 3.1. With 610 cm (20 ft) of water head, the initial trapped gas saturation is low enough that the trapped gas will not expand beyond the maximum value of 0.10 as the column is drained.

Figure 3.1 shows the gas saturation profiles in the column as a function of vertical position as it drains. (To convert to void fraction, multiply by 0.4.) The top of the column is at the right (vertical position = 610 cm [20 ft]). As liquid starts to drain from the top of the column, the gas increases from its initial value of 0.05. After 16 days (closed triangles), the gas saturation at the top of the column has risen to about 0.36, and it tapers from the top of the column to the liquid level (now at 15 feet) in a curve characteristic of partially saturated porous media. As the liquid

Table 3.1. Simulation Conditions for Case Study 1

Domain height	20 feet (160 nodes)
Initial trapped gas saturation (void fraction)	0.05 (0.02)
Drain-down time	100 days
Boundary condition type	Neumann: liquid flux = -0.35 mm/hr
Materials	Air, water, tracer gas

saturation level falls, the trapped gas at the lower vertical positions (to the left in the figure) starts to expand, leading to a gradual rise. Figure 3.2 is an expanded view of the low-saturation region of Figure 3.1. As the 100-day draining period ends (see the 96-day curve, open squares), the liquid level reaches the bottom of the column, where the trapped gas saturation is still less than 0.10 (void fraction 0.04).

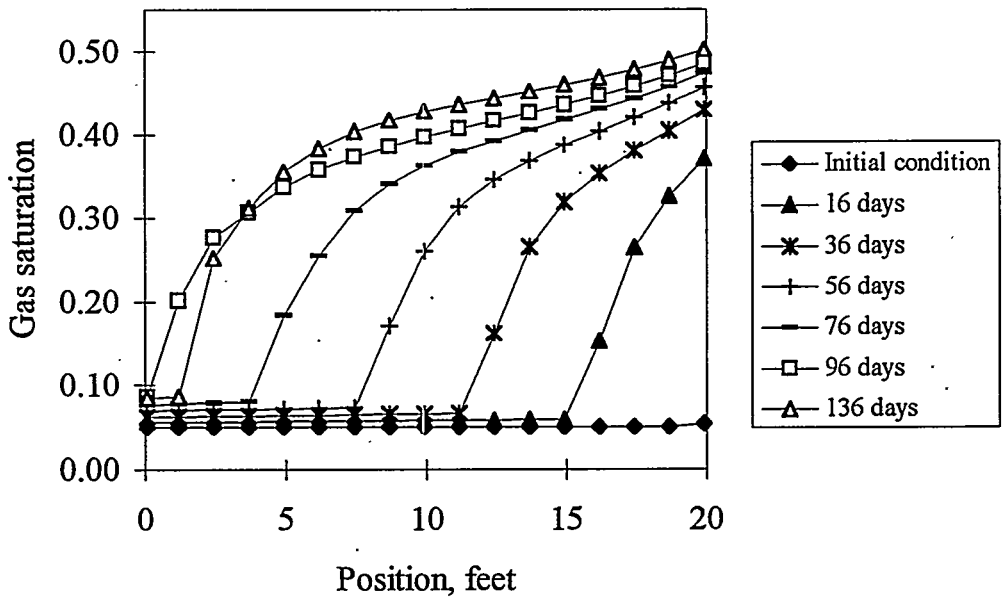

Figure 3.1. Gas Saturation Profiles for Case Study 1 (for void fraction, multiply by 0.4)

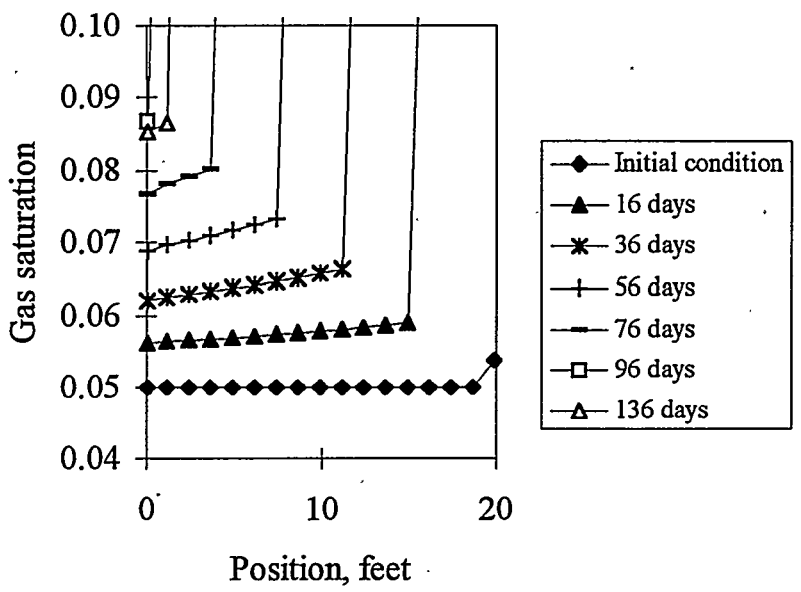

Figure 3.2. Expanded View of Figure 3.1 in Low Gas Saturation Range to Show Trapped Gas Expansion (for void fraction, multiply by 0.4)

After allowing the column to equilibrate for 40 days after the end of the draining period, some rearrangement of liquid is apparent. The gas saturation increases in the upper part of the column as liquid percolates downward into the lowest foot or so. Gas is trapped in the lowest region at a level of 0.08 to 0.09 (void fraction about 0.035). A substantial amount of liquid is still held in the column by capillary forces – more than 50% of the original liquid. This sponge-like quality of the salt cake is not surprising for porous materials with significant fine pore structure. Subsidence of the salt cake (not accounted for in the model) would likely increase the amount of liquid drained.

Figure 3.3 shows concentration profiles during draining. The trapped gas initially contains 1 mol/m^3 of the tracer gas solute. As these bubbles become connected to the air moving down from the top of the column, they are rapidly diluted, resulting in a sharp fall in concentration at the current liquid level. The solute gas then diffuses out the top of the column due to the concentration gradient. Also note that as draining progresses and the trapped gas expands, the tracer molar concentration in the trapped air falls proportionately. This effect is physical under the assumptions of the model but not in the tanks, since there is no air in those bubbles. Tank waste bubbles would expand, with some changes in gas concentrations due to soluble gases coming out of solution. Finally, at the end of the 100-day drain-down, only a small fraction of the original solute gas remains in the column. Some trapped gas, containing tracer gas in concentrations of 0.025 mol/m^3 or less, remains in the bottom quarter of the column.

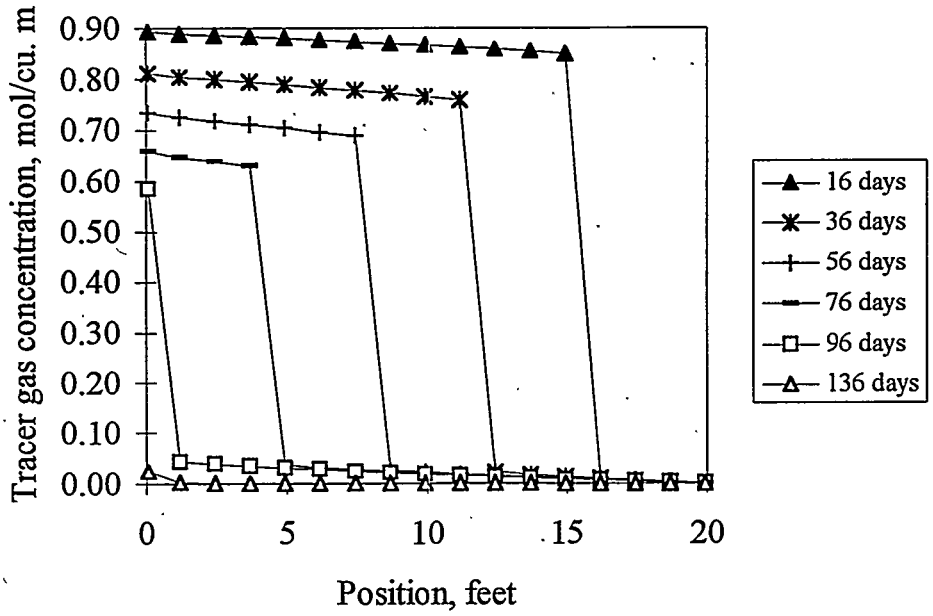

Figure 3.3. Tracer Gas Concentration Profiles for Case Study 1

As seen in Figures 3.4 and 3.5, most of the tracer gas diffuses out the top of the column during the 100-day draw-down. Figure 3.4 shows the tracer gas flux through the top surface as a function of time, while Figure 3.5 shows the same flux cumulatively. As draining begins, the tracer flux is very high. When the first few elements release their gas, the distance between those elements and the top surface is very small, and so the concentration gradient (and hence the flux) is large. The flux tapers off as the water level descends and oscillates sharply, especially early. This oscillation is a numerical artifact of the discretized model. Since tracer gas is released on an element-by-element basis, and the time for each element to open is long compared with the rate of diffusion, the tracer appears to be released in bursts. This effect decreases as the water level falls further into the column and diffusion times become longer. Increasing the node spacing (decreasing the number of elements) accentuates the effect.

From the cumulative flux graph, we see that roughly 90% of the tracer is released during the 100-day draw-down and the final 10% after draining ceases. During draining, air flows down through the upper surface of the column to fill the voids left by the receding liquid. The tracer gas must diffuse against this convective flux; however, convection is slow compared with diffusion in this case:

$$\text{(diffusion)} \gg \text{(convection)}$$

$$D_{gas}\frac{dC}{dz} \gg v_{gas}C$$

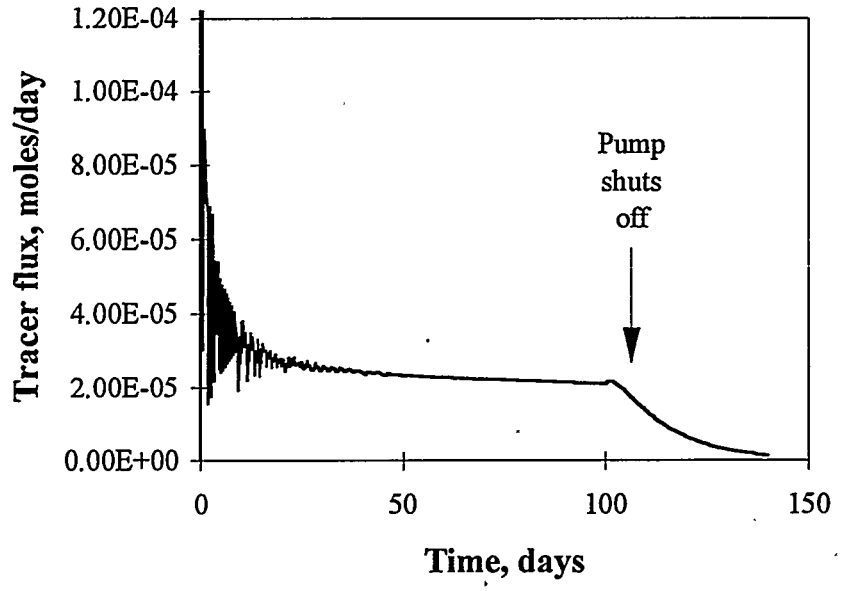

Figure 3.4. Tracer Gas Flux Through Top Surface of Column Versus Time, Case Study 1

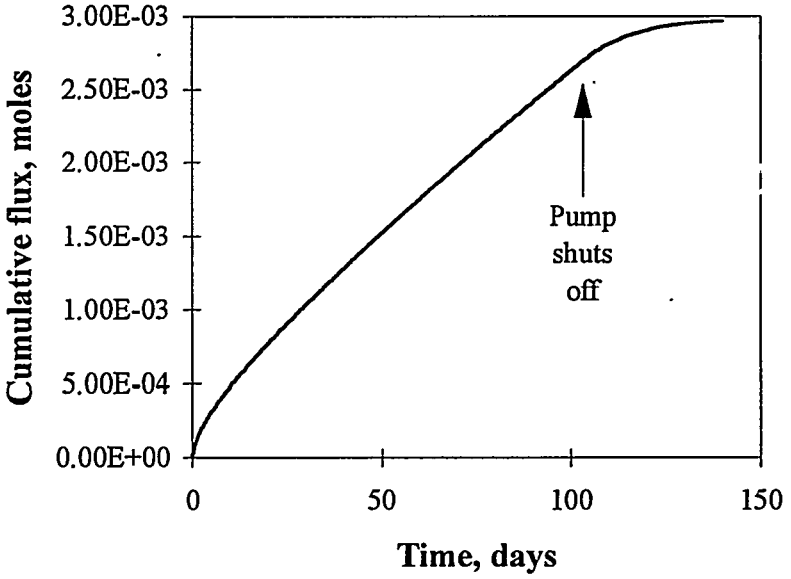

Figure 3.5. Cumulative Tracer Gas Flux Through Top Surface of Column, Case Study 1

or non-dimensionally,

$$\frac{D_{gas}}{v_{gas}L} \gg 1$$

where D_{gas} is the gas-phase diffusivity of the tracer, C is the tracer gas concentration, z is the vertical coordinate, v_{gas} is the air velocity, and L is the characteristic distance for diffusion, i.e., the distance from the top surface to the liquid level. At the beginning of drain-down, L is a few element widths; at the end, it is the height of the column. Unless v_{gas} is large (pumping very fast) or L is large (the column is very tall), diffusion can successfully compete against convection. For this case, $D_{gas} = 1\text{x}10^{-5}$ m^2/s, $v_{gas} = 9.7\text{x}10^{-8}$ m/s, and the column height is 6.1 m. Thus at the end of draining $D_{gas}/v_{gas}L = 17$, and earlier in the process it is even larger because L is smaller. However, when the pump is turned off at t = 100 days, the flux increases very slightly as the opposing convection ceases.

This is important in salt well pumping, for if diffusion cannot outpace convection during pumping, the porous salt cake will retain a substantial amount of its trapped gas. The air being drawn into the salt cake would prevent its escape. When pumping stopped, this gas would be released fairly rapidly and in an uncontrolled manner. However, when pumping is slow, diffusion allows virtually all of the gas released at any point in time to dissipate into the dome space. In this case, the gas release rate can be controlled by adjusting the pumping rate or temporarily turning off the pump. The next few case studies further illustrate this point.

3.1.2 Case Study 2: Faster Draining (10 days; 1 day)

In this case study, the drain time has been decreased from 100 days to 10 days or one day. By drawing down the water level faster, convection becomes comparable to or larger than diffusion, and the column does not desaturate as much. Table 3.2 gives the conditions for the two simulations.

Table 3.2. Simulation Conditions for Case Study 2

Domain height	20 ft (160 nodes)
Initial trapped gas saturation (void fraction)	0.05 (0.02)
Drain-down time	2a: 10 days; 2b: 1 day
Boundary condition type	Neumann: liquid flux, 2a: -2.5 mm/hr; 2b: -13.5 mm/hr
Materials	Air, water, tracer gas

Figure 3.6 shows the gas saturation profiles for the 10-day drain. During draining, the gas saturations do not rise as high as they did in the 100-day case. After the water level reaches the bottom of the tank, we allowed a 40-day equilibration period (as in Case Study 1) to allow released gas to diffuse out of the salt cake. Liquid also redistributes substantially after draining; particularly during fast draining, the liquid cannot percolate through the porous medium quickly enough to maintain an equilibrium distribution. Figure 3.7 shows the gas saturation profiles for the one-day drain, in which even less fluid is removed initially. Figures 3.8 and 3.9 show the tracer gas concentration profiles. During pumping, the concentrations in the regions above the liquid level are higher than they were in the 100-day case. Less air is entering the column to dilute the tracer (since a higher liquid saturation is retained), and it is diffusing less effectively against the incoming air. When pumping ceases and the liquid equilibrates, tracer gas clears from the region above the final liquid level.

Figures 3.10 and 3.11 show the tracer gas fluxes, instantaneously and cumulatively, for the two conditions. Much larger fractions, roughly 40 and 90%, respectively, of the released gas are retained inside the column until after the pump is turned off. With the convective gas flux now one or two orders of magnitude higher, $D_{gas}/v_{gas}L$ is now on the order of or less than 1 by the end of draining. Air is drawn into the column so quickly that the tracer cannot effectively counter-diffuse. Finally, because more of the tracer gas is retained, the total flux is progressively smaller.

It is unlikely that the tanks would ever be drained in only a few days, so most gas release is likely to be in the diffusion-dominated regime. However, in 2-D modeling, regions near the salt well itself may be subject to fast flow rates such as the ones in these examples. These cases illustrate the competing mechanisms and demonstrate that, when the assumptions above are valid, gas released from the salt cake during draining quickly diffuses into the dome space. Furthermore, since the rate of gas release is controlled by the pumping rate, the rate of gas accumulation in the dome space can be controlled by the pumping rate as well. Case Study 3 further illustrates this point.

3.1.3 Case Study 3: Pump Start and Stop

Case Study 3 further illustrates the effectiveness of diffusion in releasing gas when draining times are sufficiently long. It also shows that the liquid pump rate can be used to control the rate of gas release and accumulation in the tank dome space. In this simulation, the conditions are the same as those for Case Study 1 (see Table 3.1), but the total drain time of 100 days has been split into four 25-day stages with enough separation between them to allow all exposed gas bubbles to dissipate out of the column. Figures 3.12 and 3.13 show the instantaneous and cumulative fluxes. Notice that the tracer gas flux tails off each time pumping ceases. The tail-off time increases for each subsequent stage as the water level sinks down into the tank and the diffusion time becomes longer. However, the relative amount of gas released each time pumping ceases is small.

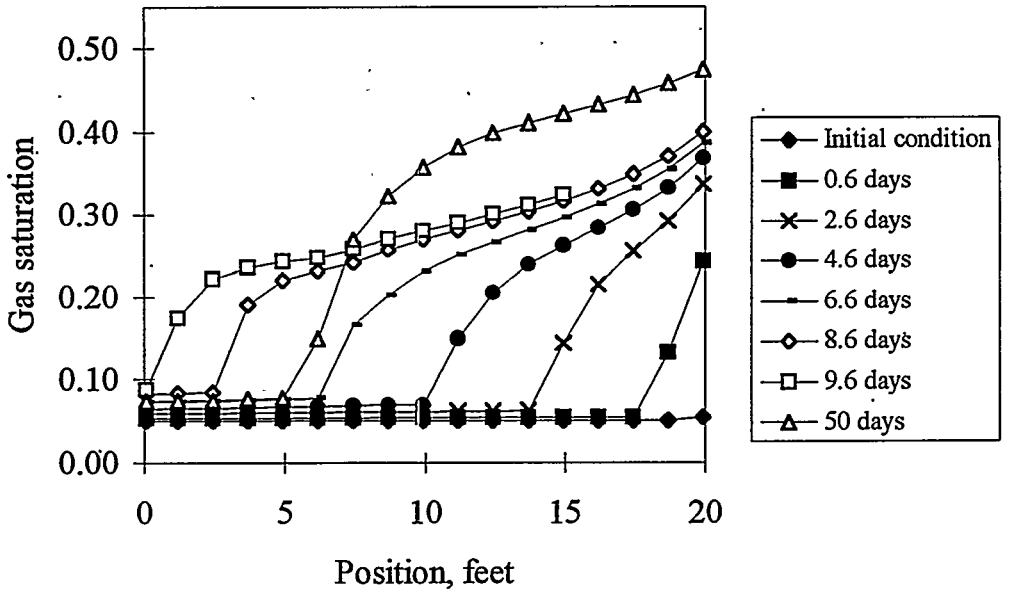

Figure 3.6. Gas Saturation Profiles for a 10-day Drain-Down (Case Study 2a) (for void fraction, multiply by 0.4)

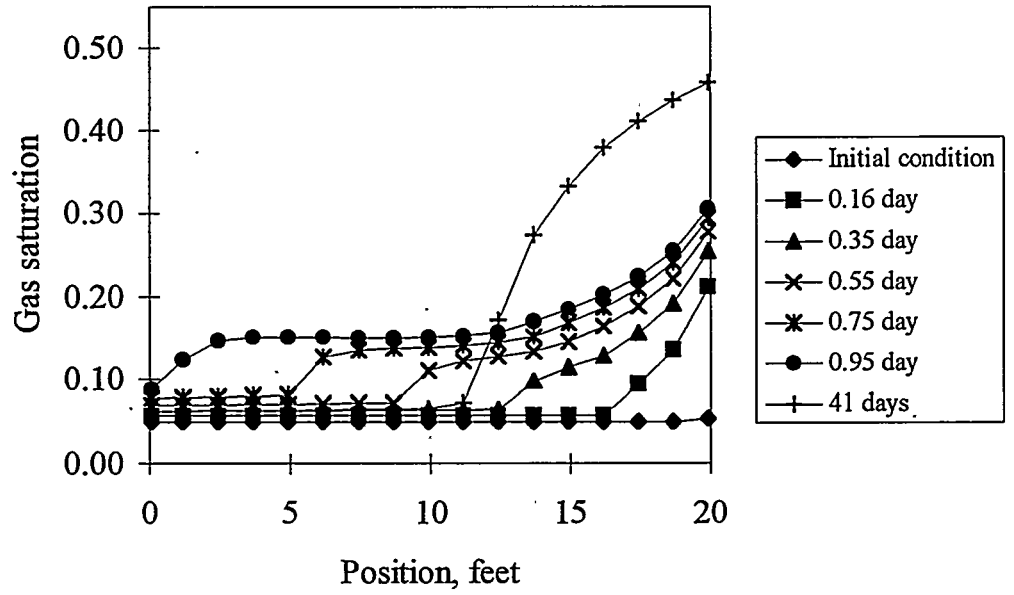

Figure 3.7. Gas Saturation Profiles for a One-Day Drain-Down (Case Study 2b) (for void fraction, multiply by 0.4)

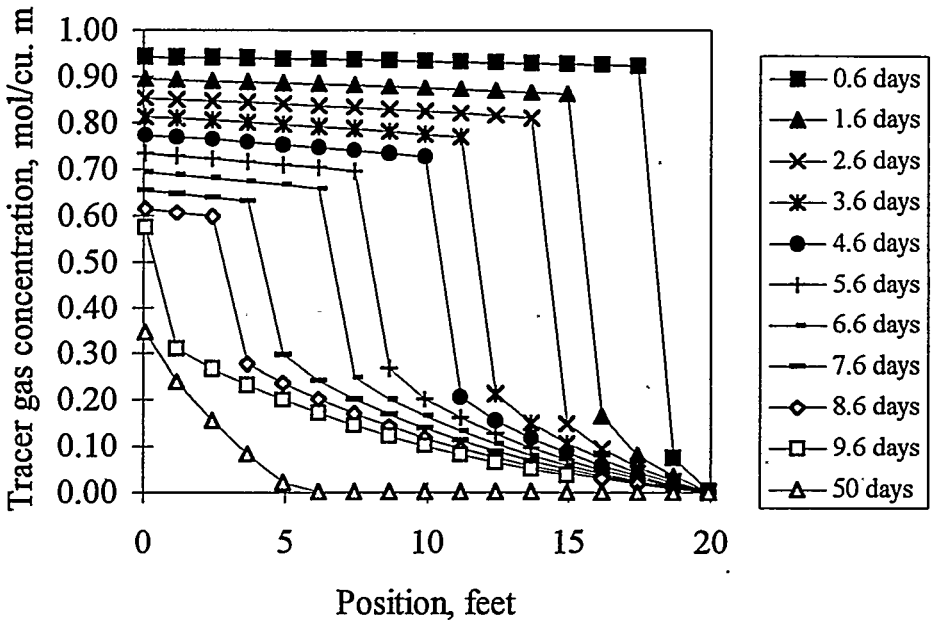

Figure 3.8. Tracer Gas Concentration Versus Position for a 10-Day Drain-Down (Case Study 2a)

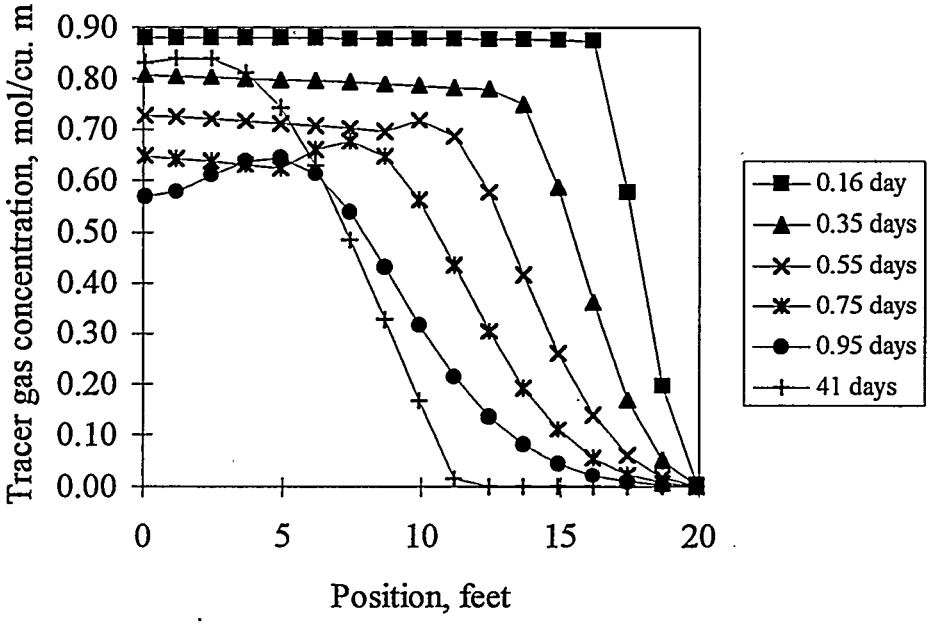

Figure 3.9. Tracer Gas Concentration Versus Position for a 1-Day Drain-Down (Case Study 2b)

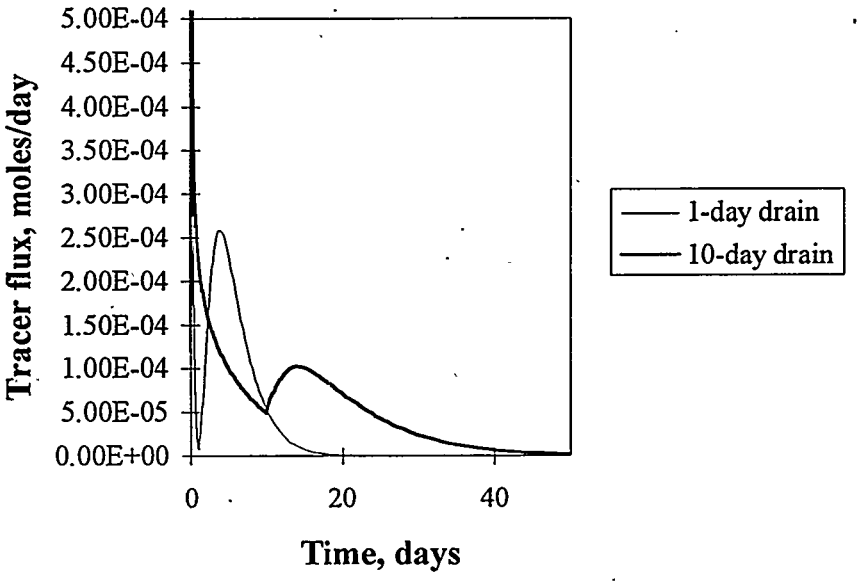

Figure 3.10. Tracer Gas Fluxes for 10-Day and 1-Day Drain-Downs (Case Studies 2a and 2b)

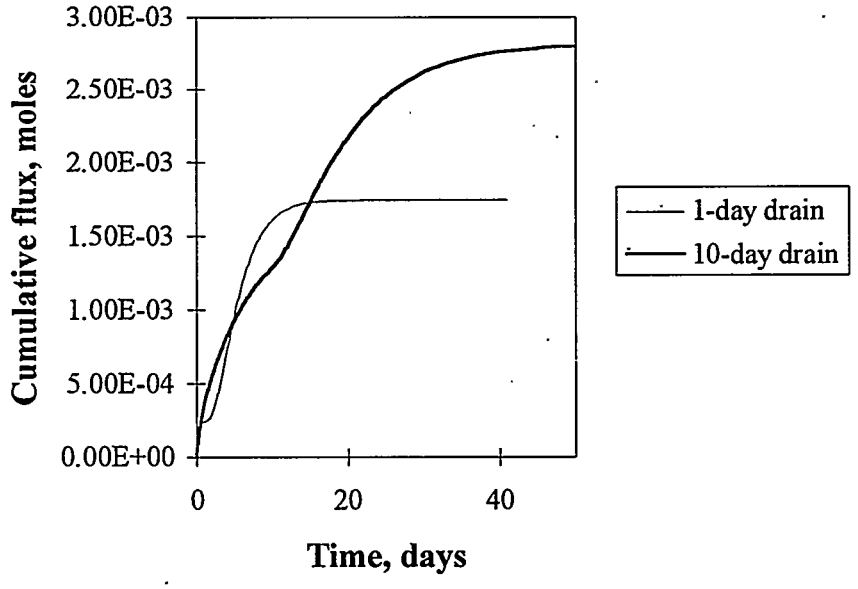

Figure 3.11. Cumulative Tracer Gas Fluxes for 10-Day and 1-Day Drain-Downs (Case Studies 2a and 2b)

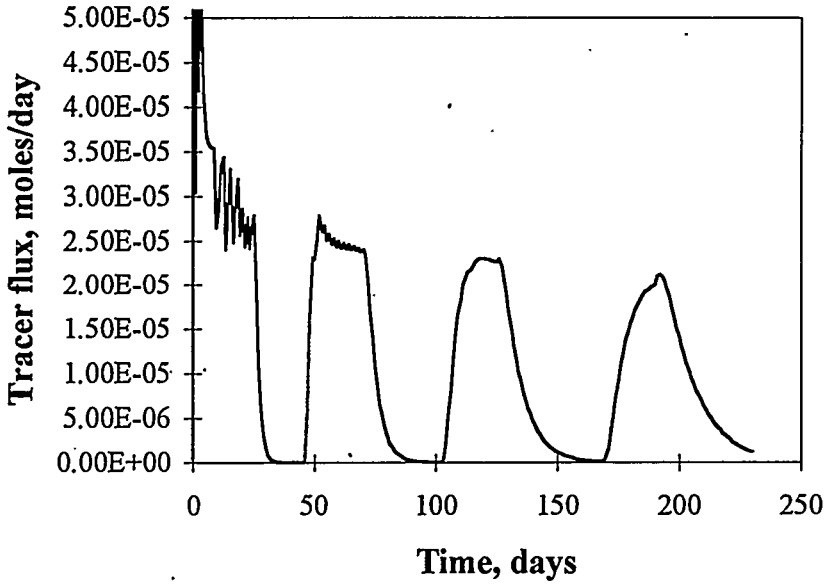

Figure 3.12. Tracer Gas Flux for Four-Stage Drain-Down (Case Study 3)

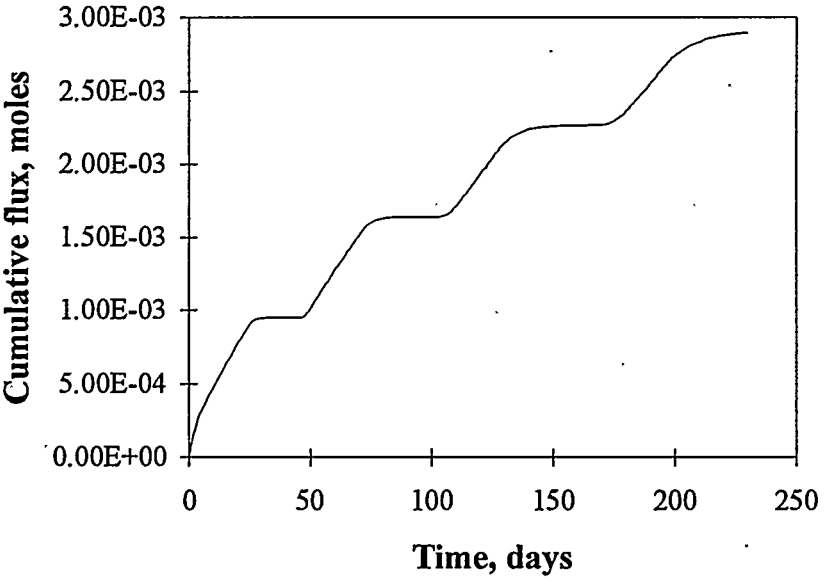

Figure 3.13. Cumulative Tracer Gas Flux for Four-Stage Drain-Down (Case Study 3)

3.1.4 Case Study 4: High Initial Gas Saturation

In the previous case studies, the initial gas saturation was 5% out of a maximum trapped gas saturation of 10% (in void fraction terms, 2% out of 4%). With a column height of 610 cm (20 ft), trapped gas at the bottom of the column expanded during drainage but not beyond the maximum value. This situation may approximate conditions in tank waste with low gas saturations where waste levels are still rising. However, in some of the tanks, the gas saturation is thought to be close to a maximum value, as evidenced by a waste level that has reached a plateau. In such waste, the trapped gas would be very close to a percolation threshold, an interconnected network of gas. Case Study 4 examines gas release behavior when the gas saturation throughout the column is near its maximum initially. (The 10% maximum trapped gas saturation is chosen somewhat arbitrarily. Depending on the details of bubble shape and solid phase structure, this value could easily be higher or lower by a factor of two.) Table 3.3 shows the simulation conditions. The domain was discretized into only 40 nodes for this case study, because model convergence was poor for smaller elements. The resulting tracer fluxes display more noise than the 160-node solutions.

The gas saturation profiles are shown in Figure 3.14. They are qualitatively similar to those for Case Study 1 (see Figure 3.1) but without the rise in gas saturation below the liquid level from 0.05 to near 0.10. Overall, the degree of desaturation is somewhat higher. However, there is no indication of fundamentally different behavior in the column, such as the development of an unstable region of high void space below the liquid level. Under the assumptions of the model, the pore spaces simply become slightly linked as the bubbles expand beyond the trapped gas maximum. With a small but finite gas phase relative permeability in these regions, gas is slowly discharged from the column through the linkages.

Figures 3.15 and 3.16 show the instantaneous and cumulative tracer gas fluxes. The instantaneous fluxes are very noisy, a numerical artifact caused by the coarse discretization of the domain. Again, approximately 90% of the gas released comes out during the 100-day draining process and 10% after draining ceases. The total amount of tracer gas released is approximately twice as high as Case Study 1 since the initial saturation was nearly double.

Table 3.3. Simulation Conditions for Case Study 4

Domain height	20 ft (40 nodes)
Initial trapped gas saturation (void fraction)	0.095 (0.038)
Drain-down time	100 days
Boundary condition type	Neumann: liquid flux, -0.35 mm/hr
Materials	Air, water, tracer gas

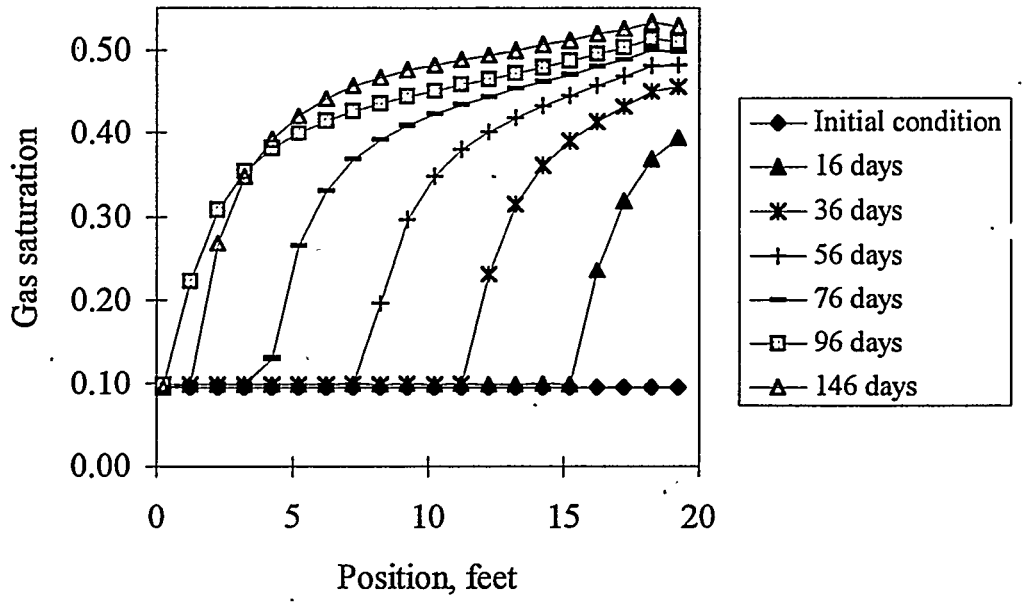

Figure 3.14. Gas Saturation Profiles for Case Study 4 (for void fraction, multiply by 0.4)

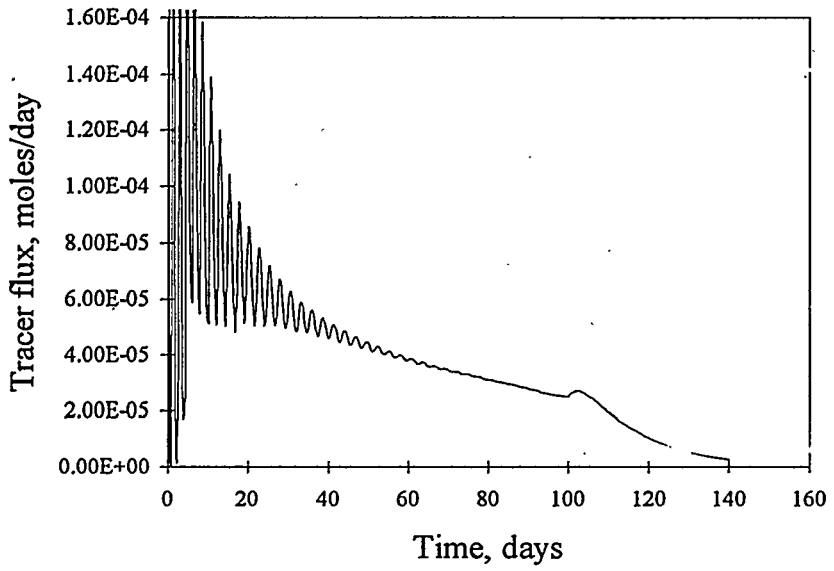

Figure 3.15. Instantaneous Tracer Gas Flux for Case Study 4 (flux noise is a numerical artifact caused by coarse discretization in this simulation)

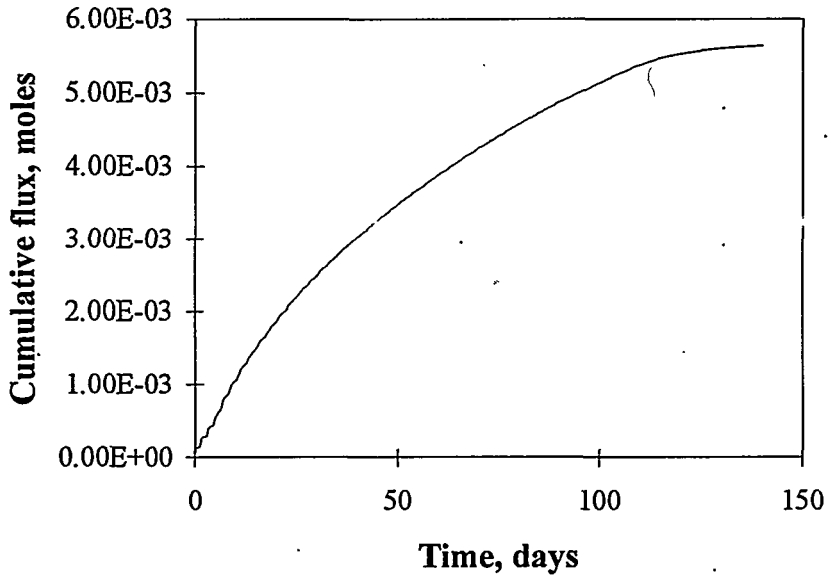

Figure 3.16. Cumulative Tracer Gas Flux for Case Study 4

For a material near the percolation threshold, then, the model predicts a slow, stable gas release, even from regions far below the surface. This prediction, while favorable from a tank waste safety perspective, should be examined critically since it relies heavily on the assumptions of the model. One of the key simplifications in the model is that the tracer gas occupies no volume. However, reductions in pressure will result in the evolution of gases dissolved in the waste, particularly ammonia. The gas saturation will therefore increase even more than simple expansion would predict. The relative increase in gas bubble volume will depend strongly on the presence of other gases, but it could be much higher than that shown here (see Appendix A for estimates and further discussion).

Even if volatilization causes bubbles to expand much more than is accounted for in STOMP, stable gas release might still result. During draining, the pressure at every point in the column is decreasing at the same rate, but the relative (fractional) pressure change is highest near the top of the undrained region. Gases would therefore be evolved most rapidly near the liquid level surface and less rapidly below. The pores could simply interlink more strongly, yielding a higher relative permeability and continuing to discharge the gas in a steady manner.

Our physical model of the waste is a permeable medium with bubbles occupying a fraction of the pore space homogeneously. If gas is retained in some other form, such as in caverns or in large fractures, our model results will not apply.

3.2 Two-Dimensional Model Results

The focus of the 2-D modeling is on predicting gas release under conditions as close as possible to actual salt well pumping. For this reason we ran the following simulations using as many of the physical properties of tank waste as are available (listed in Tables 2.1 and 3.4). Two tracer gases, one soluble and one nearly insoluble, are now included to show how their behavior differs. (Both gases are still considered to be passive tracers.) The dimensions of the simulation have been enlarged to a 23-m (75-ft)-diameter tank with a 9.1-m (30-ft)-thick salt cake layer. A second purpose of the 2-D modeling is to show radial variations in gas saturation during pumping. It is expected that the gas saturation will be higher near the central well and lower near the tank edges during draining, as depicted in Figure 1.1.

The boundary conditions for the 1-D model were set to create a constant flux of liquid out the bottom of the column. For the 2-D model, an open space was created for the well at the center of the cylindrical domain. (Actual salt well pumping will likely be from off-center risers; however, locating the well centrally simplifies modeling and interpretation.) The boundary conditions have been set so that the liquid level in the well is held constant 73 cm (2.4 ft) above the bottom of the tank, in the manner it would be during pumping. Liquid is then allowed to seep into the well along its height by applying hydraulic gradients to both the liquid and gas phases. This boundary condition does not allow the liquid removal rate to be controlled; it simply depends on the overall seepage rate, which, in turn, depends on the salt-cake permeability, the liquid viscosity, and the pressure gradient. The draining rate can therefore be expected to decay as the liquid level slowly falls. Moreover, no fixed drainage time (such as 100 days) can be applied. In practice, however, the draining (pumping) rate will be limited to 19 L (5 gal) per minute. If the liquid level in the well is set initially to a few

Table 3.4. Conditions for 2-D Simulation

Domain dimensions	Height: 9.1 m (30 ft) (40 nodes) Diameter: 23 m (75 ft) (10 nodes) Central well diameter: 30.5 cm (1 ft)
Initial trapped gas saturation (void fraction)	0.075 (0.030)
Maximum trapped gas saturation (void fraction)	0.08 (0.032)
Boundary condition type	Hydraulic gradient at well surface; liquid level fixed at 73 cm (2.4 ft) above bottom surface
Materials	Air, "tank waste" liquid phase, soluble gas, insoluble gas

feet, too large a draining rate results (when using the waste physical properties below). For this reason, the liquid level in the well is lowered from the top of the salt cake to the 73-cm (2.4-ft) level over the first 11 days of the simulation. As shown below, this gradual startup prevents the instantaneous draining rate from exceeding 19 L (5 gal)/min at any time.

The maximum trapped gas saturation for the 2-D modeling has been set to 0.08, corresponding to a void fraction of 0.032. From the safety assessment,[a] the estimated gas saturation in Tank A-101 is 7.5% (3% void), and the tank waste level is roughly constant. Since the waste volume is no longer increasing, the gas content may be at or near its percolation threshold. The selection of 8% as the maximum saturation should approximate this state and provide a conservative gas release estimate.

The initial composition of the trapped gas was set to 23 mol/m^3 insoluble tracer gas and 11 mol/m^3 soluble tracer gas. These values correspond to a bubble gas composition of 30% hydrogen and 15% ammonia, roughly that estimated for Tank A-101 in Appendix E of the safety assessment.[a] The chosen value of the equilibrium constant for the soluble gas, 5×10^{-3} (moles of solute/m^3 of gas)/moles of solute/m^3 of aqueous phase), is based on estimates for SY-101 simulants (Norton and Pederson 1994) at this gas phase concentration and equilibrium constant, the dissolved soluble gas in the waste is about 1 wt%. However, recent measurements of the ammonia content of waste in another DST, AW-101, are far lower, 0.002 to 0.004 wt%.[b] If the liquid phase soluble gas concentrations in SSTs are lower than assumed in this simulation, the predicted quantities of soluble gas released would decrease as well.

The STOMP simulation showed the tank was essentially drained after 200 days. Figures 3.17, 3.18, and 3.19 show gas saturation profiles after 10, 50, and 200 days, respectively, of pumping. (In the figures, the well is located along the y axis.) Salt cake near the well is preferentially drained to some extent, with saturation profiles tapering gradually inward, but drainage is sufficiently slow that large radial gradients do not appear to develop. At the end of pumping, gas saturations near the top of the salt cake reach approximately 65% (26% void).

Figures 3.20 and 3.21 show the amounts of gas flowing into the top of the salt cake and liquid flowing into the well as a function of time. The instantaneous rates in Figure 3.20 confirm that gradually lowering the liquid level in the well keeps the withdrawal rate below 19 L (5 gal)/min. Again, the gas inflow rate is somewhat less than the liquid outflow rate because bubble expansion fills some of the growing void volume.

(a) WHC-SD-WM-SAD-034 Rev. 0, *A Safety Assessment for Salt Well Jet Pumping Operations in Tank 241-A-101: Hanford Site, Richland, Washington* (1996) (draft).

(b) Shekarriz, A, DR Rector, MA Chieda, M White, and JM Bates. July 1996. *Retained Gas Sampler Measurement Results for Hanford Waste Tank 241-AW-101* (draft). Letter report TWSMIT-171996, Pacific Northwest National Laboratory, Richland, Washington.

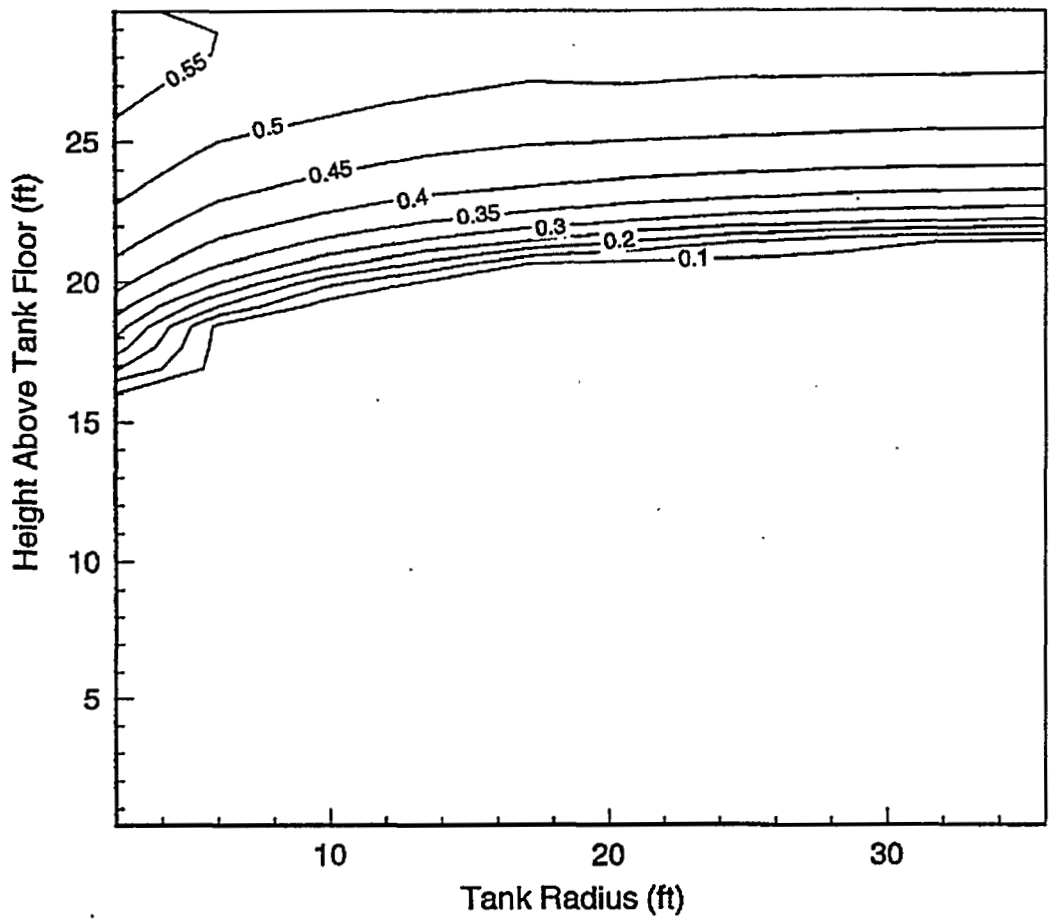

Figure 3.17. Gas Saturation Profiles After 10 Days of Salt Well Pumping (for void fraction, multiply by 0.4)

Figure 3.21 illustrates that draining is essentially complete after 200 days, when 681,372 L (180,000 gal) of liquid have been removed out of a total of 1,400,398 (370,000). The remaining liquid is trapped in the interstitial pore spaces of the salt cake, and gravity is not sufficient to pull it out. Quantitative predictions depend strongly on the parameter values chosen for the saturation function; in particular, changing the van Genuchten n parameter to a higher value (corresponding to a coarser material with a more homogeneous particle size) would result in considerably more liquid drainage. Data for characterizing the saturation behavior of salt cake are limited, and the values of these parameters are uncertain. The values chosen typify salt cake as a poorly graded sand (having a large particle size distribution). The uncertainty in the parameters makes predicting the amount of

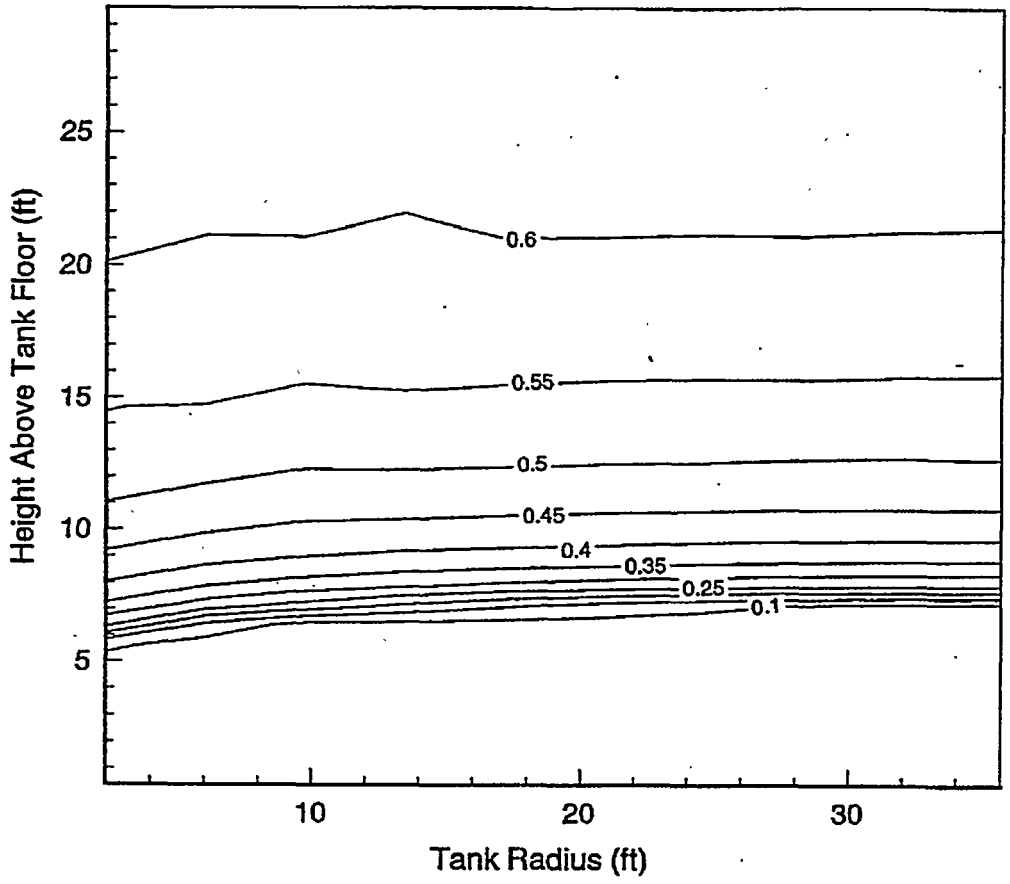

Figure 3.18. Gas Saturation Profiles After 50 Days of Salt Well Pumping (for void fraction, multiply by 0.4)

pumpable liquid difficult, and waste slumping is likely to increase the amount of liquid released. However, since salt cake is not extremely coarse (not like a gravel), a substantial fraction of the liquid will be left in the interstices, held by capillary forces. Brager (1994) predicted that out of a total of 1.5 million L (410,000 gal) of liquid in Tank A-101, 1.48 million L (390,000 gal) were pumpable.

In the simulation, draining causes rapid bubble expansion. The bubbles grow beyond the maximum value throughout the salt cake within about three days. With all of the gas space thus connected, the insoluble and soluble gases begin to diffuse through the gas phase to the top of the salt cake. Figure 3.22 shows the insoluble gas release rate as a function of time in moles per day (to convert to standard cubic feet [SCF], multiply by 0.8.) The flux is noisy at first due to the coarse discretization in the model. Figure 3.23 shows the cumulative insoluble gas release to be approximately 2500 moles, or 2000 SCF. Essentially all of the insoluble gas has diffused out of the salt cake within the first 60–100 days.

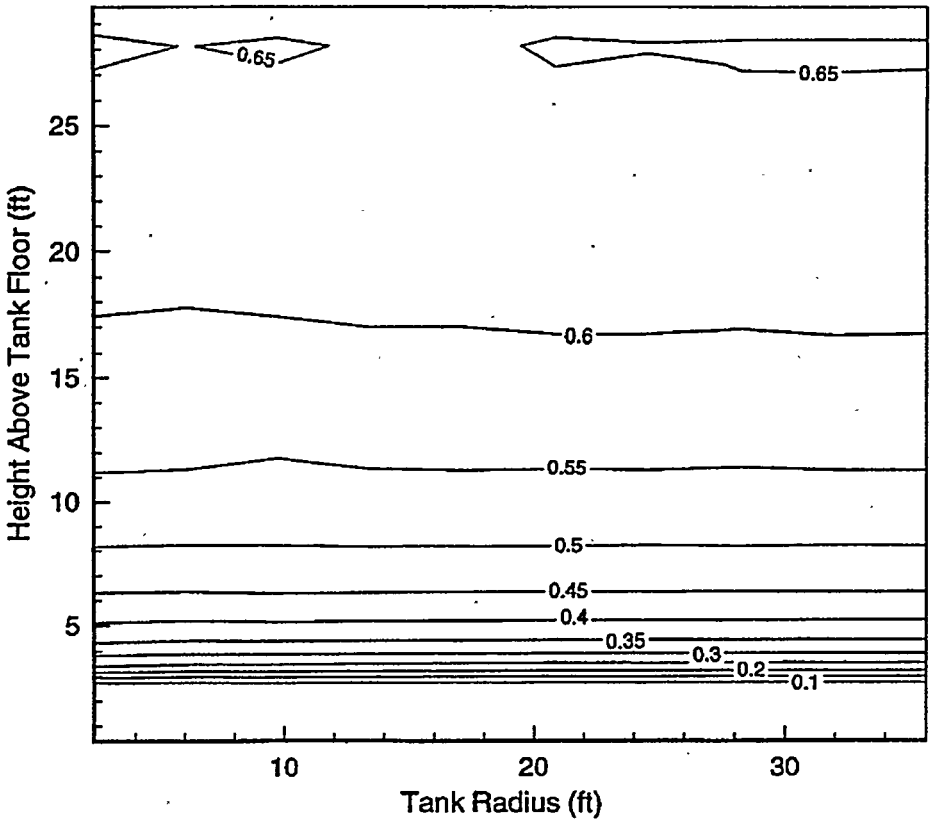

Figure 3.19. Gas Saturation Profiles After 200 Days of Salt Well Pumping (for void fraction, multiply by 0.4)

The maximum instantaneous release rate of insoluble gas was approximately 0.10 scfm, or 150 ft^3/day. Assuming a tank dome space volume of 35,000 ft^3 (Brager 1994) and a ventilation rate of 5 ft^3/min (7200 ft^3/day), the resulting dome space concentration could be about 2%. Such a release of hydrogen could potentially cause its concentration to exceed 25% of the lower flammability limit (LFL) of 6%.[(a)] However, more detailed dome space calculations would be necessary to support this conclusion.

(a) The LFL depends on the concentrations of other gases. According to the draft safety assessment (WHC-SD-WM-SAD-034 Rev. 0), Appendix G, the LFL for a retained gas mixture of 50% ammonia and 50% hydrogen has an LFL of 6.3%. However, the gas ratio may be quite different in the dome space.

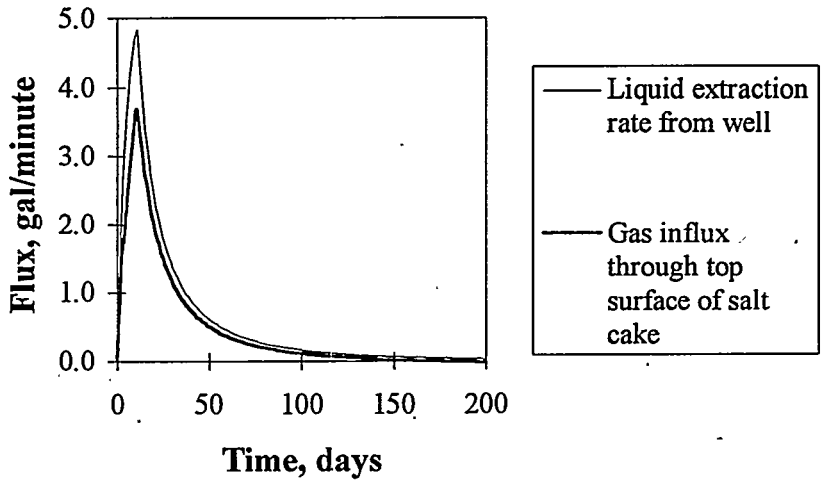

Figure 3.20. Instantaneous Gas Influx and Liquid Outflux Rates During Salt Well Pumping

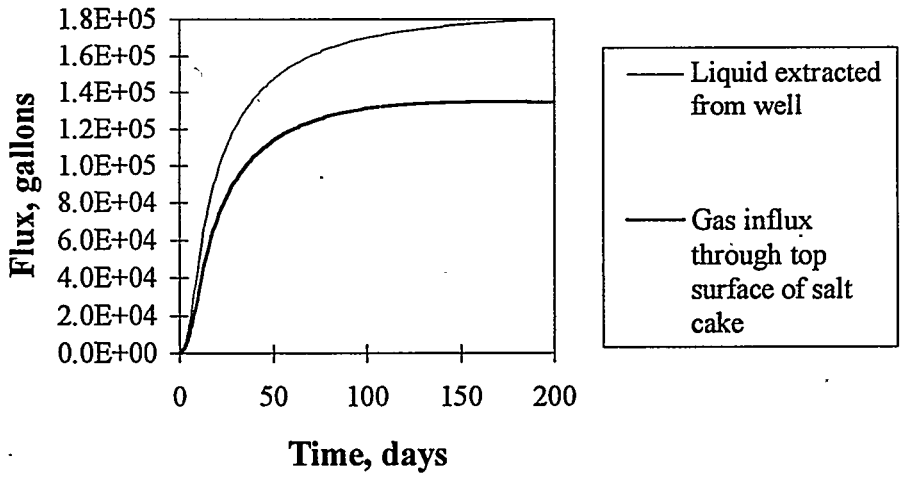

Figure 3.21. Cumulative Gas Influx and Liquid Outflux During Salt Well Pumping

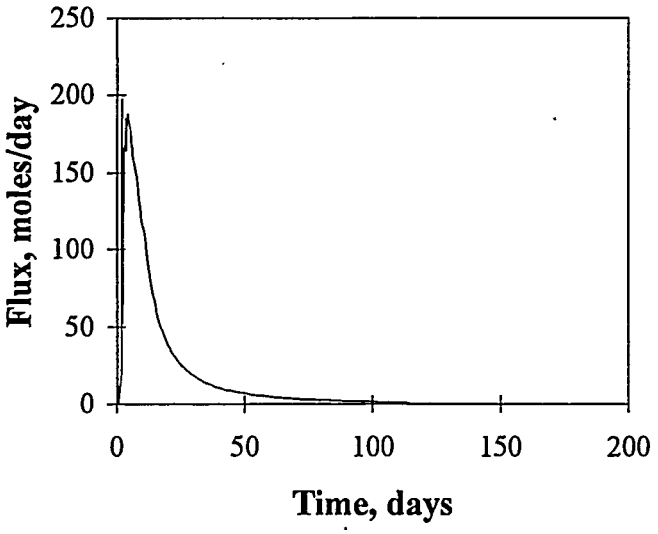

Figure 3.22. Instantaneous Insoluble Gas Release Rate Through Top of Salt Cake During Salt Well Pumping

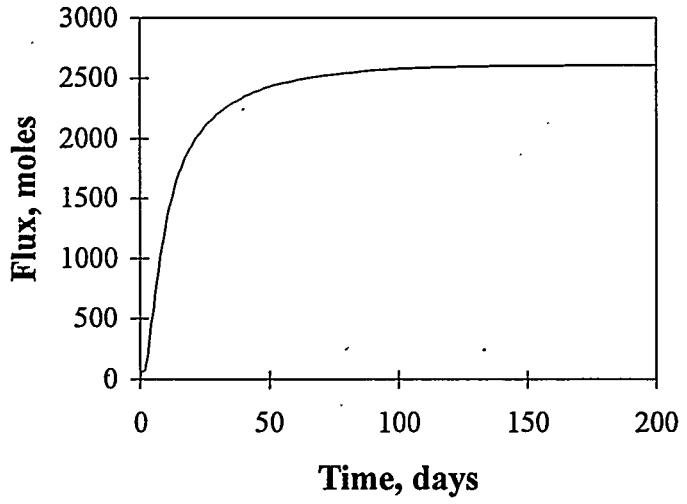

Figure 3.23. Cumulative Insoluble Gas Release During Salt Well Pumping

Figures 3.24 and 3.25 show the soluble gas release through the top of the salt cake. (Again, to convert moles to SCF, multiply by 0.8.) The flux is very large, almost 8000 moles/day early in the pumping process, and it continues at roughly 1000 moles/day long after draining is essentially complete. In the case of a soluble gas, the amount released is much higher than just the solute vapor initially in the trapped gas bubbles. As those vapors dissipate from the pore spaces in the salt cake, they are replenished by volatilization of dissolved gas. While the amounts of soluble and insoluble gas in the bubbles are initially comparable (2500 moles versus 5000 moles), there are roughly two million moles of dissolved soluble gas, or nearly 1000 times more than is initially in the gas phase. Most of that gas remains dissolved and is pumped out with the liquid phase, but a significant portion may be volatilized. Figure 3.25 shows that after 200 days, nearly 300,000 moles (240,000 SCF) of soluble gas have been released to the dome space. (Further simulation run time shows that after 500 days, the cumulative release has reached 460,000 moles, while the release rate has slowed to 450 moles/day.)

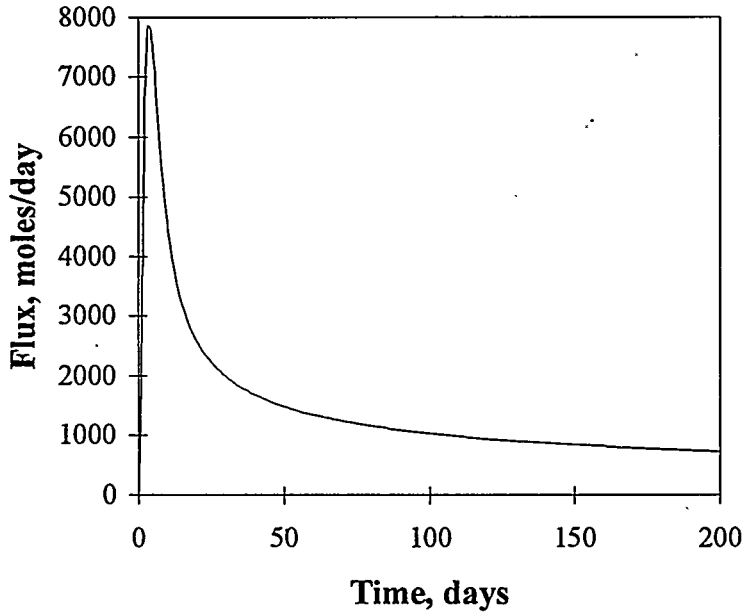

Figure 3.24. Instantaneous Soluble Gas Release Rate Through Top of Salt Cake During Salt Well Pumping

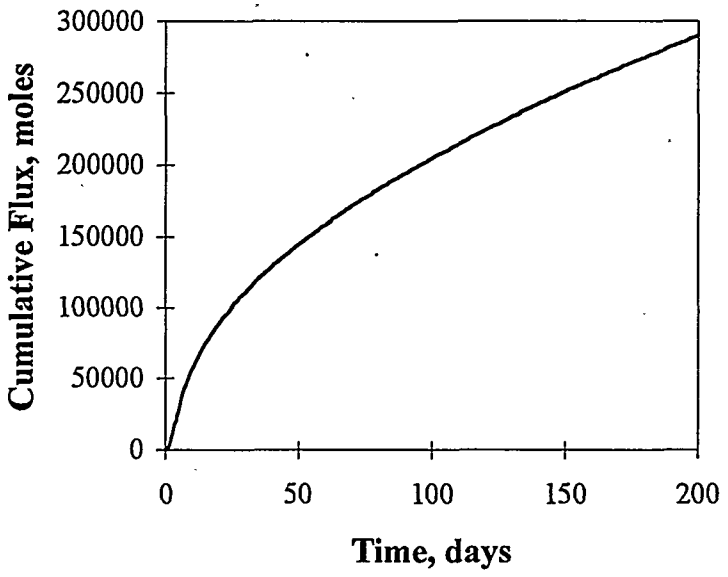

Figure 3.25. Cumulative Soluble Gas Release Through Top of Salt Cake During Salt Well Pumping

The large flux of soluble gas predicted by the simulations is an important result. Examination of the mechanisms of the model allows us to explain this conclusion, and evaluation of the model assumptions helps us to critique it. This critique is necessary because there is very little operational evidence in tank farms to support a prediction of massive ammonia release. However, the consequences of such a release are serious.

Salt well pumping causes much higher soluble gas release rates than either the slow, liquid-phase diffusion occurring before pumping or simple bubble gas release. In the simulations, gas bubble expansion and liquid level drop rapidly create a connected gas phase with an extremely high surface area for mass transfer between the liquid in the waste and the gas. Volatilization keeps the pores filled with vapor, maintaining a high driving force for diffusion. Diffusion in the gas phase is rapid compared with the liquid phase diffusion occurring in the tank before salt well pumping begins. The combination of these effects results in very high instantaneous flux rates of the volatilized gas during pumping.

Because of the equilibrium assumption in the STOMP model, replacement of vapor dissipated by diffusion is instantaneous. Since the partially drained porous medium provides intimate contact between the liquid and gas, that assumption is reasonably good. However, mass transfer limitations in the liquid phase could reduce the fluxes somewhat. Such limitations would occur if diffusion of dissolved gas from deep inside a liquid-filled pore to the gas-liquid interface were slow compared with

gas-phase diffusion out of the salt cake. Preliminary calculations have shown these rates to be comparable under the simulation conditions assuming that the contact between liquid- and gas-filled pores is reasonably fine (less than a few centimeters).

Other model assumptions bear some evaluation as well. The flux rate estimates are based on a zero-concentration boundary condition for soluble gas in the dome space, which is obviously unreasonable for a poorly ventilated dome at these high rates of release. At a (natural) ventilation rate of 5 ft^3/min (7200 ft^3/day), a release of 8000 moles/day (6400 ft^3/day) could saturate the dome space with vapor, forcing more of the soluble gas to remain in solution. Release rates would likely rise to a maximum value of the discharge rate times the saturated concentration (15%), stay constant for some period, then decay. However, detailed dome space calculations are beyond the scope of this report.

The dome space would not become pressurized by bubble gas release, because there must still be a net flux of gas into the salt cake that is comparable to the liquid drain rate. However, since STOMP does not permit solute gases to occupy any volume or exert any pressure, it is difficult to show how the air and bubble gas fluxes would really behave. At soluble gas fluxes of 8000 moles/day, or about 15 L (4 gal)/min at standard temperature and pressure, air flux into the salt cake could be considerably lower than those shown here (as in Figure 3.20), assuming no solute gas volume. This point illustrates the need for refining the STOMP model to account for solute gas volumes.

Salt cake slumping would also reduce the soluble gas flux somewhat by delaying the point in time when liquid-filled pores were exposed to gas-filled pores. STOMP does not account for changes in the volume of the medium. Dissolved gas removed during the slumping phase would reduce the amount available to volatilize later, but probably not by an order of magnitude.

To summarize the conclusions on the soluble gas release, there is consensus that volatilization and diffusion through the salt cake pores will increase dome space concentrations substantially. However, the STOMP predictions of thousands of moles per day (and ultimately hundreds of thousand of moles) may be unrealistically large. We have examined some of the model's assumptions and found reason to expect the fluxes to be somewhat less than that predicted. However, we find no glaring inconsistencies at this time. Future modeling work and future monitoring of actual pumping operations may shed additional light on this issue.

The predictions in Figures 3.22-3.25 include only gas fluxes through the top surface of the salt cake. Some gas released from bubbles may also escape through the central well. Recently, a concern was raised that hydrogen bubbles may be pumped out with the liquid, accumulating in the storage tank and posing a safety hazard. Figure 3.26 shows the STOMP prediction of 19 moles (15 SCF) of insoluble gas released into the central well during salt well pumping. Note that only a portion of the total predicted flux would be entrained in the pumped liquid. Some of the flux occurs above the liquid level in the well, and some gas released below the liquid level could bubble up through the liquid and be released.

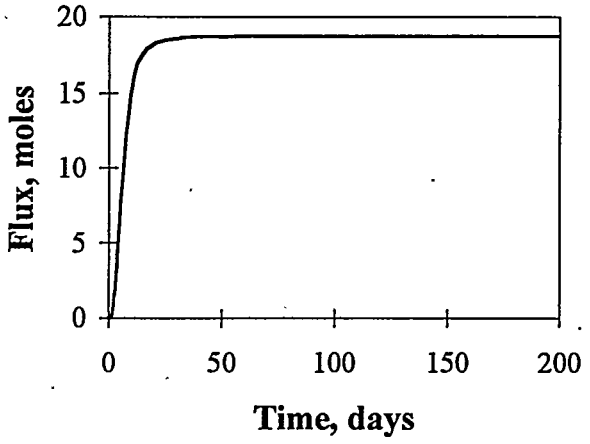

Figure 3.26. Cumulative Insoluble Gas Release Into Central Well

Finally, Figure 3.27 shows the cumulative soluble gas flux into the central well. Because of its high solubility, this flux is predominantly in the liquid phase. A total of 1.5 million moles of dissolved gas are extracted by salt well pumping compared with 0.3 million moles released into the dome space. Again, these figures are sensitive to assumptions about the saturation behavior of the waste and the amount of pumpable liquid in the salt cake.

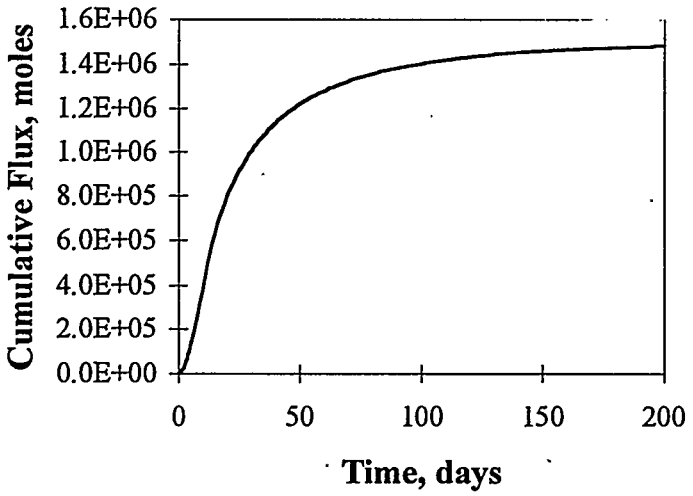

Figure 3.27. Cumulative (aqueous) Soluble Gas Release into Central Well

4.0 Model Validation Using One-Dimensional Column Experiments

STOMP is a general porous media modeling tool that includes most of the relevant physics for salt well pumping (except for increases in void fraction caused by volatilization of soluble gas). To confirm the validity of the model for salt well pumping applications, it would be best to compare its predictions with actual in-tank measurements during pumping operations. However, neither the gas concentration data nor the physical characteristics of the waste are readily available. Moreover, pumping tends to occur in a start-stop manner that does not facilitate model validation. However, model validity can also be tested in the laboratory, where the operating conditions and materials can be kept simple and well understood. (The experiments in this report involved only an insoluble gas, and so the question of the model's handling of soluble gases will be addressed in future work.)

To study the gas release phenomena typical of salt well pumping, 1-D column experiments were designed to mimic salt well pumping by draining the liquid from a bead pack containing bubbles spiked with a tracer gas. The amount of tracer gas released into the head space of the column was then measured. Experiments were performed at various draining rates (fast, medium, and slow) to investigate the regimes of diffusion- and convection-dominated transport. Because the column was relatively short, depressurization tests were also performed to mimic the loss of many feet of pressure head during salt well pumping. Thus gas release both from exposure to invading gas during draining and from bubble expansion and coalescence are investigated.

4.1 Experimental Method and Materials

Figure 4.1 is a schematic of the experimental apparatus, which consisted of a 2.54-cm (1-in)-diameter, 1.2-m (4-ft)-tall polycarbonate column filled to a height of 0.91 m (3 ft) with 1-mm glass beads to represent the permeable salt cake. (Some preliminary experiments used a 2.4-m (8-ft) tall column with a 1.8-m (6-ft) bead pack.) The column was filled with water to just above the glass beads, and trapped air bubbles were released with gentle agitation, giving a fully liquid-saturated bead pack. Gas bubbles were introduced by bubbling nitrogen containing a tracer gas, SF_6, at a concentration of 10,000 ppmv (1.01 mol%) through the bottom of the column. (During draining tests, this gas addition occurred at ambient pressure, while during depressurization experiments, the tracer gas was added at an elevated pressure of 4.5×10^5 Pa [50 psig].) SF_6 was chosen as the tracer gas because it was easily detected by an electron capture detector (ECD); release rates of the retained gas could thus be measured. The flow rate of the gas addition was controlled at 10 standard cubic centimeters per minute (sccm) with a Brooks Instrument Division 5850E flow controller. Gas addition was judged complete when bubbles could be seen flowing through the liquid level above the bead pack, indicating that the volume of retained gas in the bead pack was near its maximum. In practice, however, the volume added varied from 4-8% of the bead pack volume. A liquid-level indicator was used to measure the water volume increase as a result of the gas addition and hence

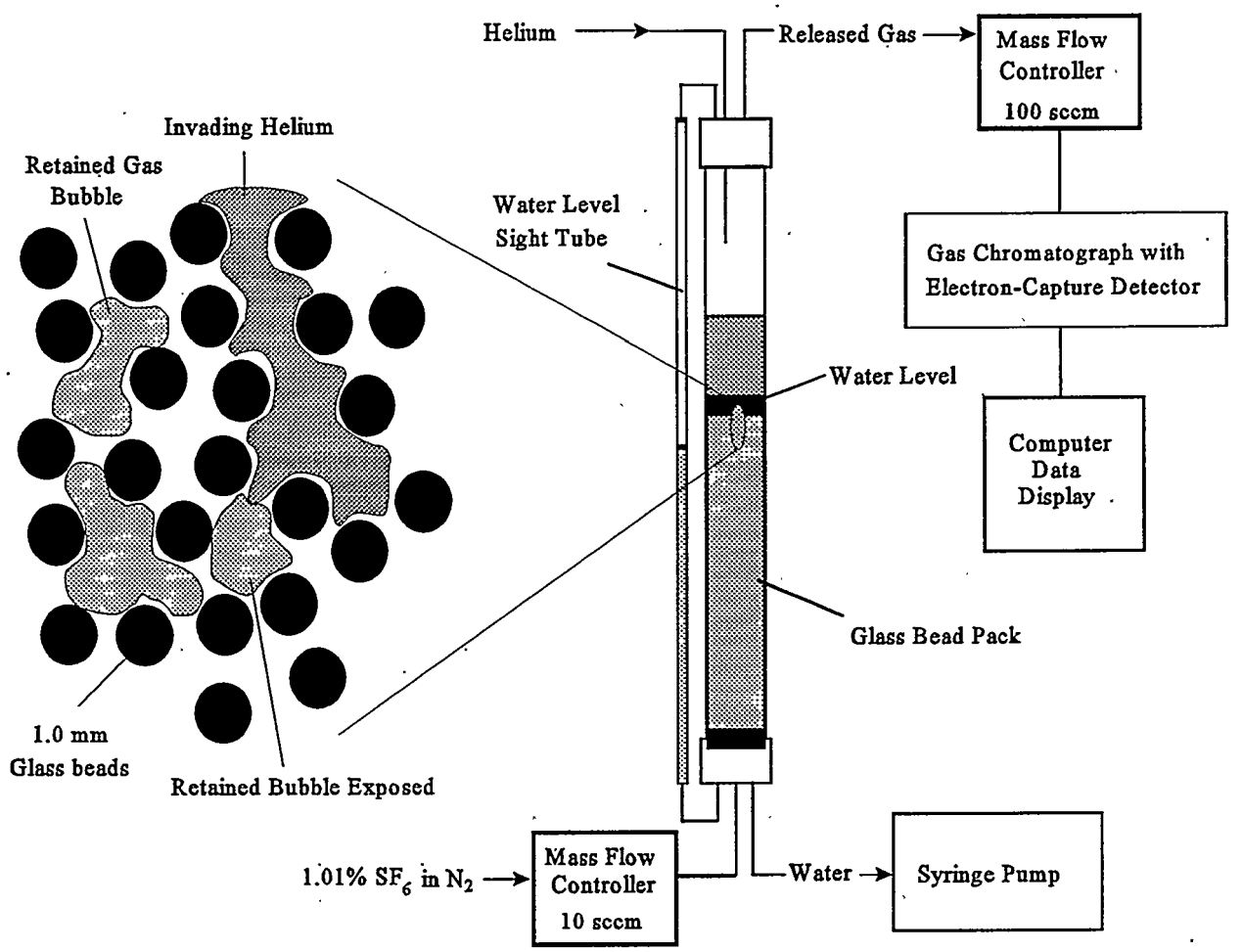

Figure 4.1. Schematic of Experimental Apparatus

the volume of retained gas bubbles in the bead pack. This measured initial amount of gas was used in subsequent mass balance calculations to determine how much of the retained gas was released during the experiments.

After gas bubbles were introduced into the bead pack, the column was pressurized (to 2.4×10^5 Pa (20 psig) during draining experiments and to 5.2×10^5 Pa (60 psig) during depressurization tests) to compress the gas bubbles. A continuous purge stream of helium (or nitrogen in some preliminary experiments) swept the headspace of the column and passed to a Hewlett Packard 5890 gas chromatograph (GC) with an ECD calibrated for SF_6. Once the headspace of the column was purged of any trace SF_6 (indicated by a negligible measurement on the ECD), the water was drained from the bottom of the column to simulate liquid draining and salt well pumping. The water drain rate was controlled using an ISCO model 500D syringe pump. Various drain rates were tested

during the experiments: a five-minute drain time (29 mL/min), a 5.5-hour drain time (0.46 mL/min), and a 54-hour drain time (0.048 mL/min). The continuous purge stream of helium or nitrogen through the column headspace then carried any released gas bubbles to the GC, which was set up to automatically inject a sample every 10 minutes and measure the concentration of SF_6 in the sample. The continuous purge stream was controlled at 100 sccm with a second Brooks Instrument Division 5850E flow controller so that the measured concentration of SF_6 on the ECD was directly proportional to the gas-bubble release rate. Draining experiments concluded when the measured amount of SF_6 was negligible (less than 1 ppbv).

Depressurization tests were also conducted where the column was slowly depressurized from 5.2×10^5 to 2.4×10^5 Pa (60 to 20 psig) at a constant rate over a one-hour period to expand the retained, unexposed gas bubbles. As before, a controlled purge stream of helium through the column headspace then carried any released gas bubbles to the GC to measure the concentration of SF_6. Depressurization tests were run using both a fully saturated bead pack (no draining) and a partially drained bead pack. Retained gas release rates for each type of experiment (fast, medium, and slow drains, depressurization without draining, and a partial fast drain followed by depressurization) were determined from the measured SF_6 concentrations and compared with those predicted by the STOMP model. These results are presented in Section 4.2.2.

4.2 Experimental Results

The experimental results are divided into two sections. Section 4.2.1 presents the experimental results from preliminary, fast draining tests that were conducted using various operating conditions to probe the mechanism of gas release and to determine the preferred operating conditions for model comparisons. In addition, a test of experimental repeatability is presented in Section 4.2.1. Section 4.2.2 compares the experimental results with model predictions. Three different draining rates were investigated: fast (5 minutes), medium (5.5 hours), and slow (54 hours). The results from the two depressurization tests are also shown. These tests were all conducted using the preferred operating conditions presented in Section 4.2.1.

4.2.1 Preliminary Results

The first preliminary tests were 5-minute drain tests conducted using either an 2.4-m (8-ft) polycarbonate column with a 1.8-m (6-ft) bead pack or a 1.2-m (4-ft) polycarbonate column with a 0.91-m (3-ft) bead pack. The rate of SF_6 released during these two tests is compared in Figure 4.2. The plots are presented on a logarithmic scale because, following the peak concentration, the flux decreases with a constant slope over the logarithmic scale, allowing the two rates to be easily compared. Time zero in Figure 4.2 is the onset of draining. As discussed in Section 3, during rapid draining the diffusion rate of gas from exposed bubbles is slower than the convection rate of invading gas. Figure 4.2 shows that there was no significant gas release during draining (0–5 minutes). Once draining stopped, however, the exposed bubbles were easily released by diffusion.

Figure 4.2 shows that the SF_6 release rate (i.e., the retained gas release rate) achieved with the 0.91-m (3-ft) bead pack was significantly faster than the rate achieved with the 1.8-m (6-ft) bead

pack. This result agrees with our understanding of gas release controlled by gas-phase diffusion once draining ceases. A doubling of the packing height should cause a four-fold increase in the decay time, since the diffusion time scales with the square of the path length. For convenience, all subsequent experiments performed for model validation were conducted using the 1.2-m (4-ft) column with a 0.91-m (3-ft) bead pack.

In Figure 4.2, the peak SF_6 concentration differs in the two tests because a less concentrated tracer (100 ppmv SF_6 in nitrogen compared to 10,000 ppmv) was used in the 1.8-m (6-ft) bead pack test. The dip in SF_6 concentration in the 1.8-m (6-ft) test was caused by a temporary increase in the helium purge flow rate.

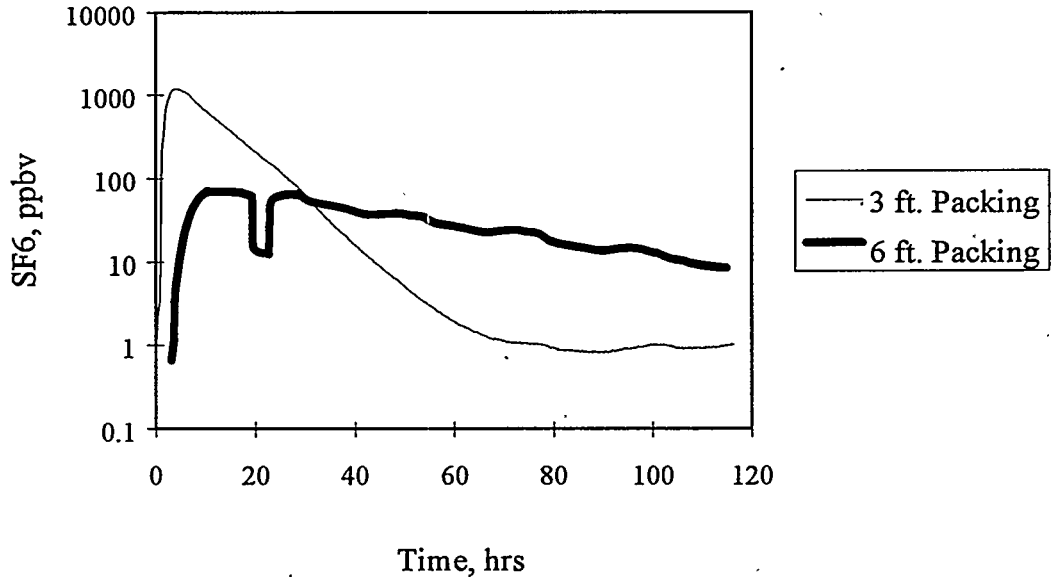

Figure 4.2. Effect of Bead Pack Length in Preliminary Fast Draining Experiments

The second operating condition tested during the preliminary experiments was the purge gas. During draining, the purge gas invades the pores of the packing and becomes the gas phase against which the tracer gas must diffuse to escape the column. The rate of diffusion will therefore depend on the binary diffusivity of the purge gas-tracer gas mixture. The results from experiments using nitrogen or helium are presented in Figure 4.3. Both tests were conducted with the 0.91-m (3-ft) bead pack. (The data for helium are the same as those in Figure 4.2.) As before, time zero is the onset of draining, and the plots are presented on a logarithmic scale so that the two rates can be easily compared. The noise in the nitrogen data is due to the daily heating and cooling that occurred in the high bay, where the experiments took place.

Figure 4.3 shows that when helium is the invading gas the retained gas release rate is much faster than when nitrogen is the invading gas. Again, this test validates our understanding of gas phase diffusion as the release mechanism. The diffusivity of SF_6 against helium is five times greater than against nitrogen (0.174 cm^2/s compared with 0.0348 cm^2/s).[(a)] A five-fold decrease in gas diffusivity should increase the decay time by a factor of 5. Again, for convenience, subsequent experiments performed for model validation were conducted using helium as the invading gas.

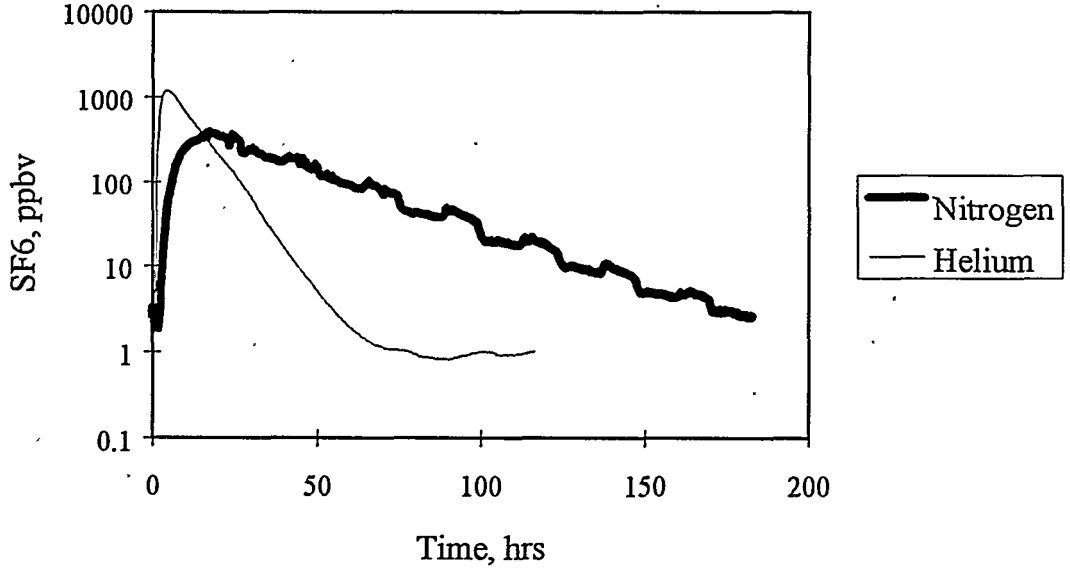

Figure 4.3. Effect of Invading Gas in Preliminary Fast Draining Experiments

(a) Diffusivities estimated using Leonard-Jones parameters as presented in Reid et al. (1977).

Operating conditions were duplicated for several experiments to ensure that the results were repeatable. Figure 4.4 shows data from two different tests conducted using the 1.2-m (4-ft) column with a 0.91-m (3-ft) bead pack and helium as the invading gas. The data for "Test 2" are the same data presented above in Figures 4.2 and 4.3 for the 0.91-m (3-ft) packing and helium as the invading gas. As Figure 4.4 shows, the experiments were fairly repeatable. The peak flux in Test 2 was about 30% higher than in Test 1. After 40 hours, when Test 1 was interupted, the flux was a factor of two higher than in Test 1.

4.2.2 Comparing Experimental Results with Model Predictions

In this section we compare column experiment data and predictions from the STOMP model. All experiments were performed using the preferred operating conditions of a 3-ft (91-cm) bead pack and helium purge gas. Except as noted, all the input parameters for the simulations were the same for the various tests. To represent the new porous medium, a 1-mm bead pack, the input parameters selected were different from those used in the 1-D tests in Section 3. These new values are listed in Table 4.1.

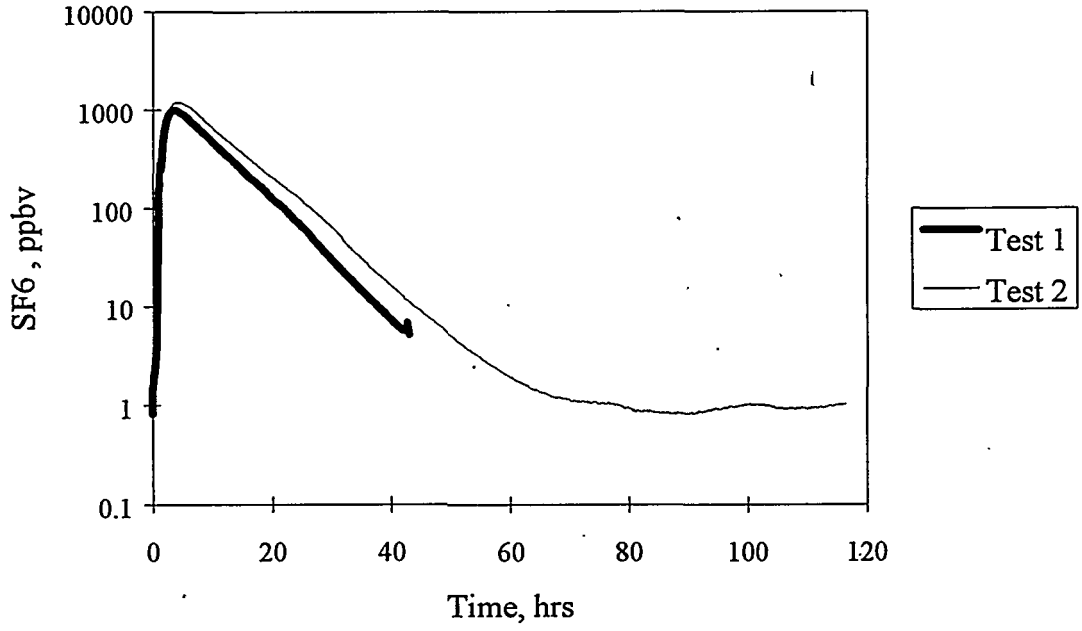

Figure 4.4. Repeatability of Data from Experiments Using a 3-ft Bead Pack and Helium

Table 4.1. Physical Parameters Used in the STOMP Simulations for Model Validation

Parameter	Value	Units	Source/Basis
Hydraulic conductivity	10^4	Darcy	See discussion in text
van Genuchten alpha parameter	drainage: 8 imbibition: 12	1/m	Dullien (1992)
van Genuchten n parameter	8	unitless	Dullien (1992)
Residual liquid saturation	0.08	unitless	Dullien (1992)
Initial trapped gas saturation (void fraction)	drain: 0.042 (0.017) dp: varies	unitless	One constant, approximate value used for modeling draining experiments; measured value used for modeling depressurization experiments
Maximum entrapped air saturation (void fraction)	drain: 0.10 (0.04); dp: 0.18 (0.072)	unitless	Draining simulations used a value that was likely too low; see discussion in text
Gas phase diffusivity, 1 atm	0.397	cm^2/s	Reid et al. (1977)
Gas-aqueous partition coefficient	10^{10}.	m^3 aq/m^3 gas	SF_6 treated as essentially insoluble
Tortuosity	0.67	unitless	Dullien (1992). Note STOMP definition is inverse of standard definition.

All of the input parameters for STOMP, such as those in Table 4.1, were independently measured or estimated. (STOMP has no parameters that are simply adjusted to fit its predictions to experimental data.) The values of the van Genuchten alpha and n parameters, which describe the capillary behavior of the porous material, were based on data in Dullien (1992) for bead packs. The tortuosity, which took the default value of 1.0 for the results in Section 3, was also taken from Dullien (1992). The hydraulic conductivity was set higher than expected, but this value was chosen to reflect the actual draining behavior of the bead pack during the experiments. When modeling the fast draining test, setting the input hydraulic conductivity to a lower value (several thousand darcy) did not allow the liquid to drain freely. Instead, a significant "rebound" in the water level occurred after draining, as liquid from the top of the column continued to infiltrate to the bottom. This rebound effect was not observed experimentally. This behavior is characteristic of a high permeability medium, so the permeability was increased in the model.

The fast, medium, and slow draining rate tests were modeled using an initial void fraction of 4.2% (1.7% void) and a maximum trapped gas saturation of 10% (4% void). These values were chosen based on initial observations of how much gas could be added to the column before it would

begin to break through. Later observations showed that higher initial gas saturations were possible, as much as 18%. For the depressurization tests, measured initial values of the gas saturation were used for each simulation, and the maximum trapped gas saturation was specified as 18%.

The STOMP model predicts fluxes based on an artificial initial tracer gas concentration, while the experiment measures SF_6 concentration in a purge stream. The two sets of data have therefore been normalized to either the same peak concentration or the same cumulative amount released, as noted. The flux scales shown are therefore nominal.

With these adjustments, predictions of gas release rates were generated for all of the cases described below. The agreement between experiment and model was generally good.

4.2.2.1 Fast Draining Rate

Figures 4.5 and 4.6 compare the experimental data from the 5-minute drain with model predictions. The data are presented as instantaneous flux (equivalent to a gas release rate) versus time (Figure 4.5 in linear form and 4.6 in a semi-log version). In all results presented, the beginning of draining is designated as time = 0.

The agreement between the data and the model results was good. The time of peak flux out of the column was slightly later in the experimental data. Figure 4.6 shows that, following the peak, the flux decreases with a constant slope over the logarithmic scale, indicating exponential decay. (Exponential decay is typical of diffusion-controlled processes such as this one.) The data and the model were in good agreement on the slope in that region of exponential decay, i.e., the rate constant. The data leveled off after about 60 hours, because the GC-ECD reached its SF_6 detection limit of about 1 ppb.

Calculating the cumulative amount of SF_6 measured by the GC over the course of a test yields an estimate of the total amount of the trapped gas released. The initial amount of gas present in the column was also measured for each test. One can therefore compute the measured fractional release and compare it with that predicted by the model. This comparison could serve as another check on model validity. Typically, however, such a "mass balance" (the amount of gas accounted for at the end of each experiment) is not very repeatable. Table 4.2 shows the measured cumulative SF_6 released and the predicted values for each of the experiments in this section. For all of the draining tests, the model predicted that virtually all of the SF_6 was released. The experimental results ranged from 27% to 120%. While this range seems to be large, it is not unusual for measurements of this type. It should be noted that the primary data used for comparison are the release rate data; the cumulative recovery data were used mainly as tools to determine whether the experimental results were acceptable. In some cases, seemingly good experiments had order-of-magnitude errors in cumulative recovery, presumably due to system leaks, and these experimental results were rejected.

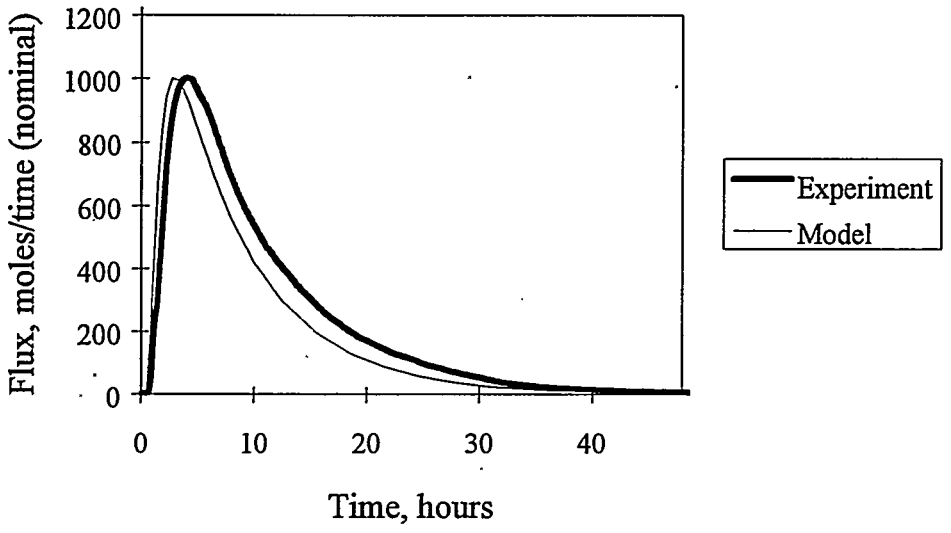

Figure 4.5. Experimental and Predicted SF_6 Flux, 5-Minute Drain (linear scale)

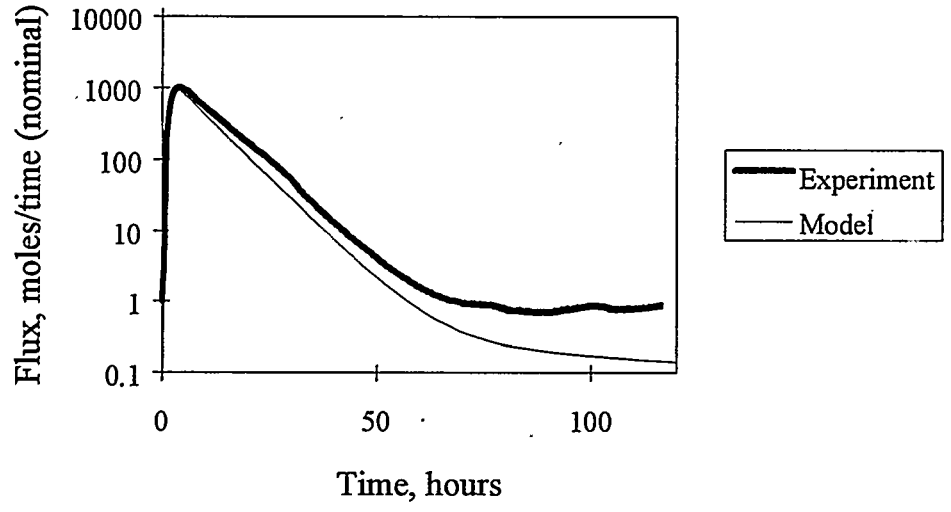

Figure 4.6. Experimental and Predicted SF_6 Flux, 5-Minute Drain (semi-log scale)

Table 4.2. Measured Versus Predicted Cumulative Release of SF_6 During Validation Experiments

Experiment	Gas Released, Measured	Gas Released, Predicted
Fast	73%	100%
Medium	120%	100%
Slow	103%	100%
Depressurization	35%	39.5%
Drain/Depressurize/Drain	27%	100%

4.2.2.2 Medium Draining Rate

In the medium draining rate experiments, the column was drained in 5.5 hours. Figures 4.7 and 4.8 compare the experimental data with the model predictions for this case. Again, the data are presented as nominal flux versus time (Figures 4.7 and 4.8, linear and semi-log, respectively). These data are normalized so that the peak height is 1000 units for both curves.

In the medium draining rate case, the rate of diffusion of gas from exposed bubbles competed evenly with the rate of invading gas. Therefore, about half of the gas escaped during draining, the other half was released once draining stopped. The data and model results are in good qualitative agreement, but the relative peak heights are not the same. The experimental data showed that relatively more gas was released after draining stopped. As in the 5-minute drain case, the concentration reached its peak later in the data than in the model results.

For this experiment, the GC indicated that the total amount of SF_6 released from the column exceeded the amount originally added by 20%. This again illustrates the uncertainty in the experimental cumulative data. The model showed 100% release.

4.2.2.3 Slow Draining Rate

Figures 4.9 and 4.10 show the data for the slow draining rate case, a 54-hour drain. In the slow draining scenario, the rate of diffusion of gas from exposed bubbles is faster than the rate of invading gas, and therefore about 90% of the gas that is released does so during draining. The data for this case was noisy and includes a large, unexplained dip (assumed to be part of the experimental noise), but the agreement with the model results was still good. As shown in Figure 4.10, the data and the model were in good agreement on the rate at which the flux decayed exponentially (the slope between 50 and 90 hours). As noted in Table 4.2, the cumulative release measured was several percent beyond 100%.

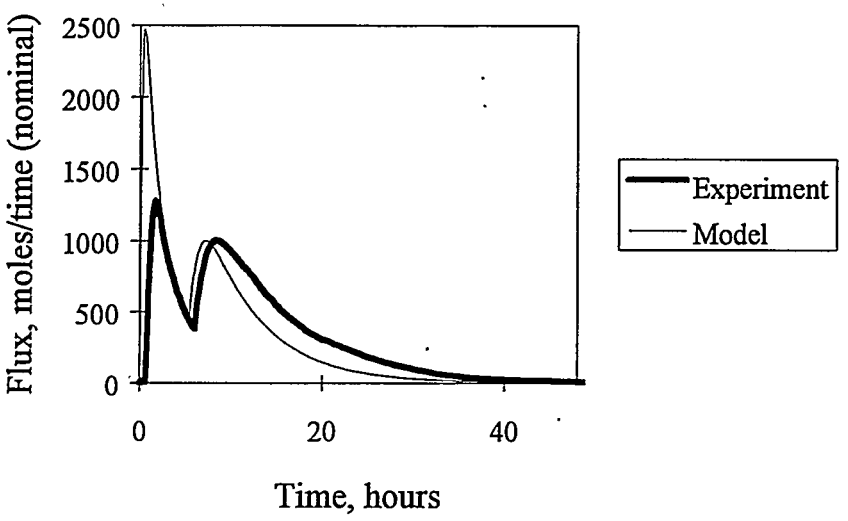

Figure 4.7. Experimental and Predicted SF_6 Released, 5.5-Hour Drain (linear scale)

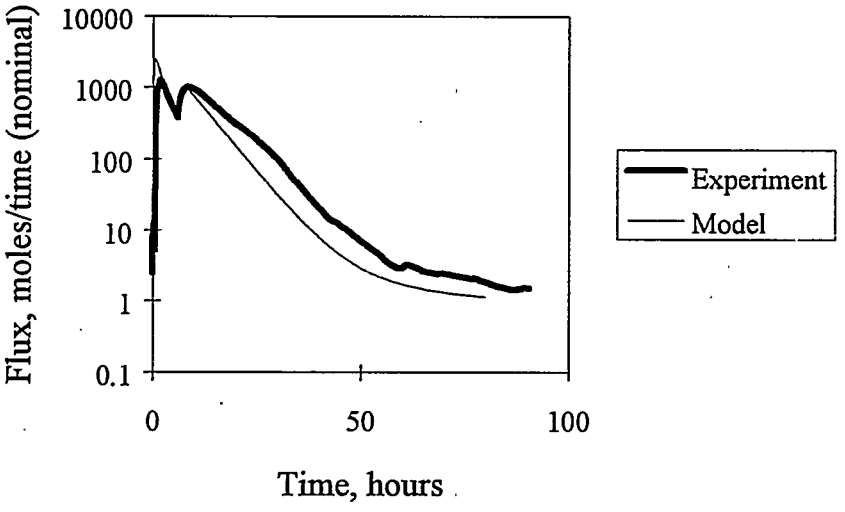

Figure 4.8. Experimental and Predicted SF_6 Released, 5.5-Hour Drain (semi-log scale)

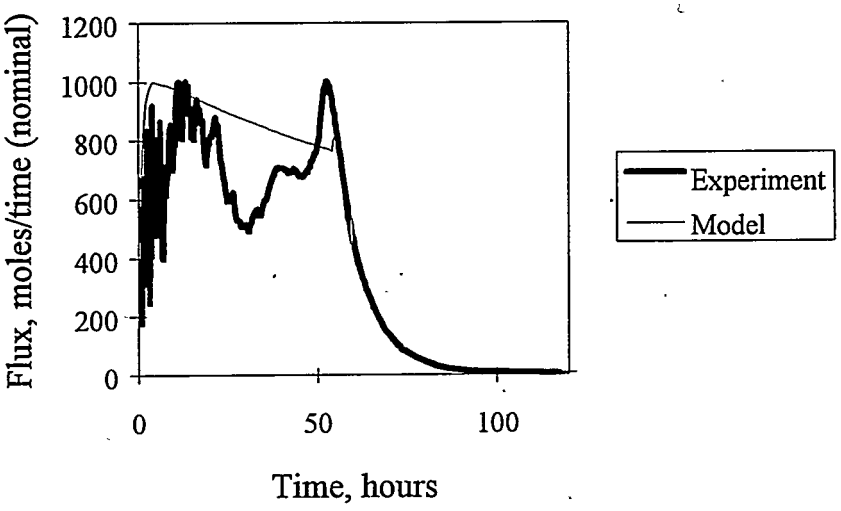

Figure 4.9. Experimental and Predicted SF_6 Released, 54-Hour Drain (linear scale)

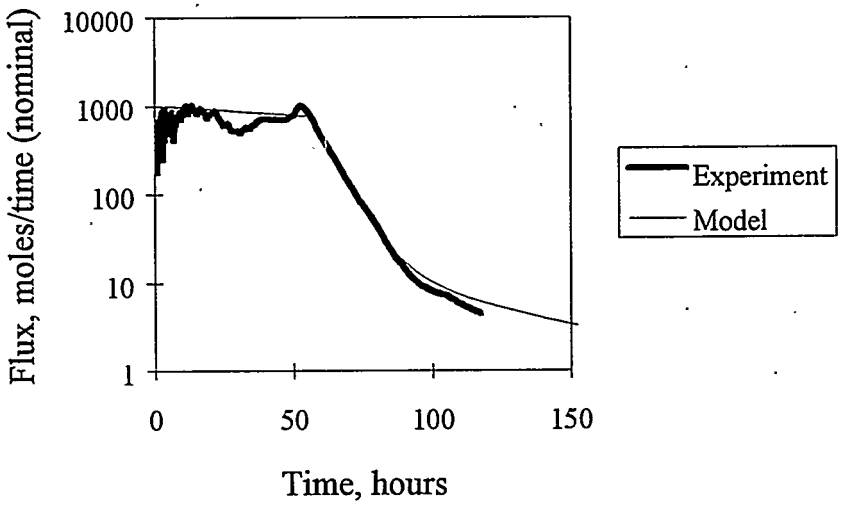

Figure 4.10. Experimental and Predicted SF_6 Released, 54-Hour Drain (semi-log scale)

4.2.2.4 Depressurization Test

In the draining tests, the packed column was only 3 ft tall. The total change in hydrostatic head on the trapped gas during the experiment was therefore small, roughly 10% of the ambient pressure at the bottom of the column. In comparison, gas near the bottom of the tank could experience a pressure reduction of 50 to 70% during actual salt well pumping, and as a result bubbles could double or triple in size, potentially interconnecting and releasing gas. To study this regime, we conducted tests in which the column was loaded at an elevated pressure and then slowly depressurized, allowing gas bubbles to swell and escape. The results were compared with model predictions simulating the same changing conditions.

In the first such test, gas was injected into the column at 446 kPa (50 psig) and then compressed to 515 kPa (60 psig). The pressure was then slowly lowered to 239 kPa (20 psig) over one hour. The initial gas saturation at 50 psig was measured to be 12.5% (5% void). The maximum trapped gas saturation was set to 18% (7.2% void) in the model, in accordance with recent observations of how much gas could be added. The resulting SF_6 flux out of the column is shown in Figure 4.11 and compared to the STOMP prediction. Pressure versus time is shown on the secondary axis.

The test shows that initially no gas was released. As the pressure fell to about 343 kPa (35 psig), however, gas began to evolve from the column. Once the pressure leveled off at 239 kPa (20 psig), the flux quickly decayed. The model and our observations of the experiment allow us to interpret these results. Recall that the column is loaded by injecting gas into the bottom at 446 kPa (50 psig) until bubbles begin to break through the top of the packing. At that time, channels of interconnecting bubbles are thought to span the height of the column. Turning off the gas flow causes the bubbles to snap off at pore throats, disconnecting them slightly. Then, pressurizing the column from 446 to 515 kPa (50 to 60 psig) compresses the bubbles somewhat, making the breaks between bubbles larger. As depressurization begins, however, the bubbles do not necessarily expand only in the direction that connects them again along their previous path; rather, they can move out into nearby pore spaces, especially small ones. The result is that the channels of gas bubbles do not interconnect until the pressure is significantly less than 446 kPa (50 psig) (at 0.25 hours), as seen in Figure 4.11.

The measured gas flux is much noisier for this test than it was in the draining experiments. This noise is caused by episodic releases of groups of bubbles, which are clearly visible during the test. The model does not reflect this noise, since it treats the trapped gas as a uniform gas saturation generating a gradual release, not as bubbles.

The measured percent release for this experiment was 35%, shown in Table 4.2. The STOMP model predicted a release of 39.5%.

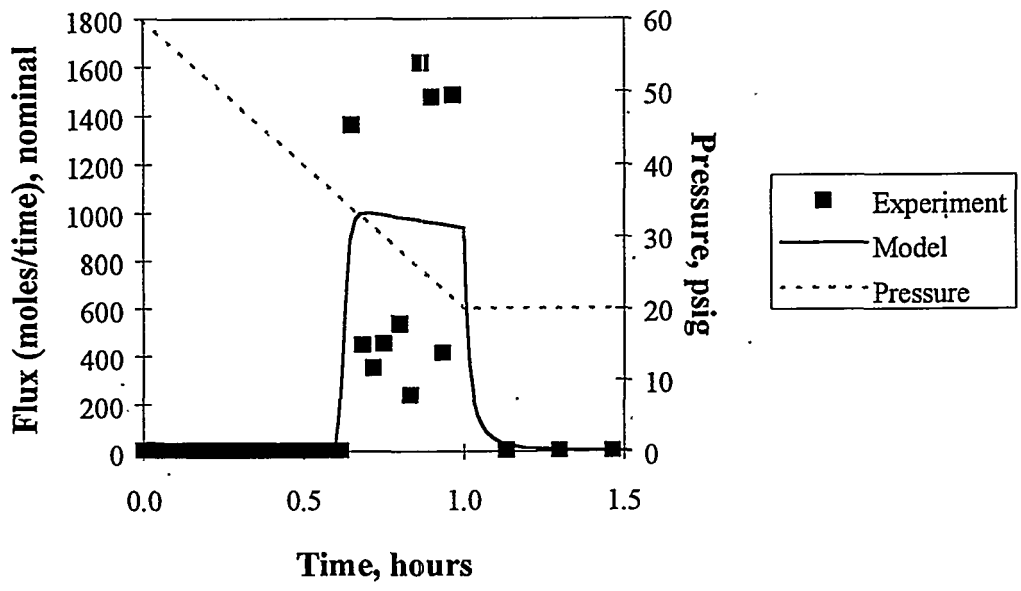

Figure 4.11. Comparison of Experimental and Predicted SF_6 Released, Depressurization Test

4.2.2.5 Partial Drain Followed by Depressurization and Drain

In this test, the column was loaded at 446 kPa (50 psig) and pressurized to 515 kPa (60 psig), as in the depressurization test. Then it was drained in the manner of the draining tests above, but only until the liquid level fell by half the column height. Gas evolved slowly from the column for about 45 hours. The pressure was then lowered from 60 to 20 psig over 45 minutes. Gas was allowed to evolve for about 18 hours, and then the column was drained to the bottom. Figure 4.12 shows the measure gas flux and the accompanying model prediction on a semi-log scale, with the ambient pressure on the secondary axis. The model results were normalized so that the peak heights are approximately matched.

The results show the same behavior after each operation. The fast initial drain (the first five minutes in Figure 4.12) results in a large flux that decays exponentially, as SF_6 clears from the upper half of the column for 45 hours. Depressurization over 45 minutes (a relatively small amount of time on the scale of the chart) results in another flux that decays away for 18 hours. To end the test, quickly draining the second half of the column produces a final peak and that subsequently decays. The data and model are in good agreement on predicting ratios of the peak heights, and the rates of decay are also approximately the same.

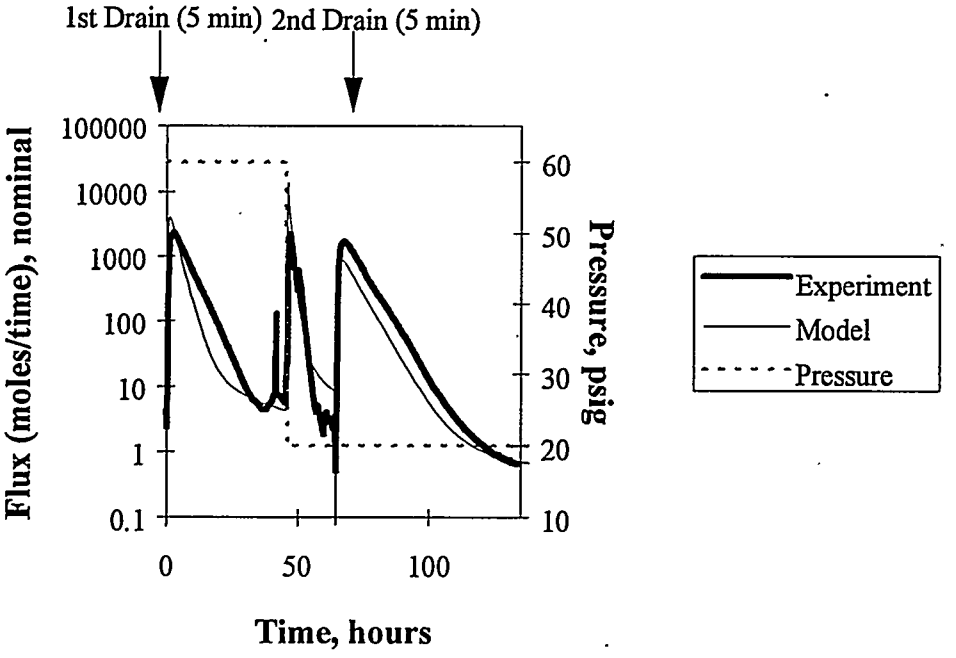

Figure 4.12. Comparison of Experimental and Predicted SF_6 Released, Partial Drain/Depressurization/Partial Drain Test

4.3 Model Validation: Conclusions

The agreement between the experimental results and the model predictions was quite good. The correct qualitative behaviors were seen. First, the effect of lengthening the column or changing the carrier gas was verified, indicating that gas-phase diffusion is, in fact, the dominant transport mechanism after draining stops. Second, the decay of the gas flux was shown to be exponential, and the model matches the exponential decay constants well. Third, the depressurization test showed that STOMP correctly handles bubble expansion caused by decreasing pressure. In both experiment and model, gas began to evolve only once the bubbles interconnected. Good qualitative agreement supports the use of the model as a tool for understanding gas release during salt well pumping.

Quantitatively, the model tended to under-predict the peak time during the fast draining experiments and over-predict the exponential decay constant slightly in general. The ratio of the two peak heights for the medium-rate draining test was off by about a factor of two. Otherwise, the model predictions were also quite good quantitatively, supporting its use for predicting gas release amounts during salt well pumping. However, this model validation was limited to release of insoluble gas. Further validation should be done to evaluate STOMP's handling of soluble gases under salt well pumping conditions.

5.0 Summary and Conclusions

These are our conclusions from modeling salt well pumping:

- Approximately half of the liquid in the salt cake is pumpable; when liquid is pumped from the bottom of the tank, half drains by gravity and half is retained in the interstices of the pores.

- Draining the pumpable liquid from the salt cake releases essentially all of the insoluble gas. Using the assumed characteristics of Tank A-101, 56.6 m^3 (2000 SCF) of insoluble gas are released over the course of 60 to 100 days. The maximum release rate was 4.25 m^3 (150 ft^3)/day. Depending on the ventilation rate and the amounts of other gases present, such a release could cause the hydrogen concentration in the dome space to exceed 25% of the LFL.

- While most of the soluble gas is withdrawn with the pumped liquid, a large quantity (as much as 11,327 m^3 (400,000 SCF) could be volatilized and released into the dome space. Instantaneous release rates are as high as 181 m^3 (6400 ft^3)/day. These results seem high compared with operational experience and are based on several assumptions, including a very large ventilation rate. A limited ventilation rate would result in a dome space saturated with vapor and a lower vapor release rate. Mass transfer limitations in the liquid phase and salt cake slumping could also reduce release rates.

- Essentially all the gas in bubbles is released when exposed by invading gas (i.e., when the liquid level falls below that region). If the gas saturation is near its percolation threshold, some trapped gas is released from below the liquid level as bubbles expand, but just enough to maintain the material at its percolation threshold. Gas release is slow and steady rather than sudden and dramatic.

- When the rate of liquid withdrawal is small, about 100 days, diffusion of gas from exposed bubbles is far faster than the convection of invading air into the salt cake. As a result, gases released from trapped bubbles quickly diffuse through the drained portion of the salt cake and into the dome space. In this situation, there is little accumulation of bubble gases in the drained portion of the salt cake. The release rate of gas is proportional to the draining rate, and the cessation of pumping quickly reduces the release rate to zero. However, a small increase in the release rate occurs when pumping ceases because in the absence of inward flow of air, the gas in exposed bubbles releases more effectively by diffusion.

- When the draining rate is fast, about one day, the diffusion rate of gas from exposed bubbles is slower than the rate of invading gas. In this situation, there is negligible diffusion upwind against the invading gas and therefore no release during draining. However, when the liquid draining ceases, the previously trapped gas is easily released by diffusion, giving a larger-than-expected release rate.

- Little insoluble gas (less than 15 SCF) is released into the well during pumping.

These are our conclusions from the model validation tests:

- The agreement between the experimental results and the model predictions was good. First, lengthening the column or changing the carrier gas had the effect of demonstrating that gas-phase diffusion is the dominant transport mechanism except during fast draining. Second, the gas flux was shown to decay exponentially, and the model matched the exponential decay constants well. Third, the depressurization test showed that STOMP correctly handles bubble expansion caused by decreasing pressure.

6.0 References

Brager, HR. 1994. *Summary of Information on the Flammable Gas Watch List Tanks.* WHC-EP-0711, Westinghouse Hanford Company, Richland, Washington.

Bredt, PR, and SM Tingey. 1996. *The Effect of Dilution on the Gas Retention Behavior of Tank 241-SY-103 Waste.* PNL-10893, Pacific Northwest National Laboratory, Richland, Washington.

Bredt, PR, SM Tingey, and EH Shade. 1995. *The Effect of Dilution on the Gas-Retention Behavior of Tank 241-SY-101 Waste.* PNL-10781, Pacific Northwest Laboratory, Richland, Washington.

Dullien, FAL. 1992. *Porous Media: Fluid Transport and Pore Structure.* Academic Press, San Diego.

Gauglitz, PA, SD Rassat, PR Bredt, JH Konynenbelt, SM Tingey, and DP Mendoza. 1996. *Mechanisms of Gas Bubble Retention and Release: Results for Hanford Waste Tanks 241-S-102 and 241-SY-103 and Single-Shell Tank Simulants.* PNNL-11298, Pacific Northwest National Laboratory, Richland, Washington.

Gauglitz, PA, SD Rassat, MR Powell, RR Shah, and LA Mahoney. 1995. *Gas Bubble Retention and its Effect on Waste Properties: Retention Mechanisms, Viscosity, and Tensile and Shear Strengths.* PNL-10740, Pacific Northwest Laboratory, Richland, Washington.

Gauglitz, PA, LA Mahoney, DP Mendoza, and MC Miller. 1994. *Mechanisms of Gas Bubble Retention.* PNL-10120, Pacific Northwest Laboratory, Richland, Washington.

Grimes, GW. 1978. *Jet Pump Development for Salt Well Application.* RHO-CD-316, Rockwell Hanford Operations, Richland, Washington.

Handy, LL. 1975. *Flow Properties of Salt Cake for Interstitial Liquid Removal/Immobilization Development Program.* ARH-C-6, Atlantic Richfield Hanford Company, Richland, Washington.

Hanlon, BM. 1995. *Waste Tank Summary Report for Month Ending August 31, 1995.* WHC-EP-0182-89, Westinghouse Hanford Company, Richland, Washington.

Hodgson, KM, RP Anantatmula, SA Barker, KD Fowler, JD Hopkins, JA Lechelt, and DA Reynolds. 1995. *Evaluation of Hanford Tanks for Trapped Gas.* WHC-SD-WM-ER-526 Rev. 0, Westinghouse Hanford Company, Richland, Washington.

Hodgson, KM, RP Anantatmula, SA Barker, KD Fowler, JD Hopkins, JA Lechelt, DA Reynolds, DC Hedengren, RE Stout, and RT Winward. 1996. *Evaluation of Hanford Tanks for Trapped Gas.* WHC-SD-WM-ER-526 Rev. 1, Westinghouse Hanford Company, Richland, Washington.

Hopkins, JD. 1995. *Methodology for Flammable Gas Evaluations.* WHC-SD-WM-TI-724, Westinghouse Hanford Company, Richland, Washington.

Kubic, WL Jr. 1995. *Summary, Review, and Analysis of Data for Tank 241-A-101.* Los Alamos National Laboratory Report TSA10-CN-WT-SA-DA-001, Los Alamos, New Mexico.

Lenhard, RJ, and JC Parker. 1987. "A Model for Hysteretic Constitutive Relations Governing Multiphase Flow 2. Permeability-Saturation Relations." *Water Resources Research* 23: 2197-2206.

Metz, WP. 1976. *A Topical Report on Interstitial Liquid Removal from Hanford Salt Cakes.* ARH-CD-545, Atlantic Richfield Hanford Company, Richland, Washington.

Norton, JD, and LR Pederson. 1994. *Ammonia in Simulated Hanford Double-Shell Tank Wastes: Solubility and Effects on Surface Tension.* PNL-10173, Pacific Northwest National Laboratory, Richland, Washington.

Parker, JC, and RJ Lenhard. 1987. "A Model for Hysteretic Constitutive Relations Governing Multiphase Flow 1. Saturation Pressure Relations." *Water Resources Research* 23: 2187-2196.

Rassat, SD, and PA Gauglitz. 1995. *Bubble Retention in Synthetic Sludge: Testing of Alternative Gas Retention Apparatus.* PNL-10661, Pacific Northwest Laboratory, Richland, Washington.

Reid, RC, JM Prausnitz, and TK Sherwood. 1977. *The Properties of Gases and Liquids,* 3rd Edition. McGraw Hill, New York.

Shepard, CL, CW Stewart, JM Alzheimer, TI Stokes, G Terrones, G Chen, and NE Wilkins. 1995. *In Situ Determination of Rheological Properties and Void Fraction: Hanford Waste Tank 241-SY-103.* PNL-10865, Pacific Northwest Laboratory, Richland, Washington.

Simmons, CS. 1995. *Modeling Water Retention of Simulant Sludge and Actual Salt Cake Tank Wastes.* PNL-10831, Pacific Northwest Laboratory, Richland, Washington.

Stewart, CW, JM Alzheimer, ME Brewster, G Chen, RE Mendoza, HC Reid, CL Shepard, and G Terrones. 1996. *In Situ Rheology and Gas Volume in Hanford Double-Shell Tanks.* PNNL-11296, Pacific Northwest National Laboratory, Richland, Washington.

Stewart, CW, CL Shepard, JM Alzheimer, TI Stokes, and G Terrones. 1995. *In Situ Determination of Rheological Properties and Void Fraction in Hanford Waste Tank 241-SY-101.* PNL-10682, Pacific Northwest Laboratory, Richland, Washington.

Strachan, DM. 1975a. *Permeability, Capillarity, and Pore Volume of Synthetic Hanford Salt* Cake. ARH-ST-129, Atlantic Richfield Hanford Company, Richland, Washington.

Strachan, DM. 1975b. *Effect of Carbon Dioxide on the Permeability of Synthetic Hanford Salt* Cake. ARH-ST-130, Atlantic Richfield Hanford Company, Richland, Washington.

Welty, JR, CE Wicks, and RE Wilson. 1984. *Fundamentals of Momentum, Heat, and Mass Transfer, 3rd Edition.* John Wiley and Sons, New York.

Whitney, P. 1995. *Screening the Hanford Tanks for Trapped Gas.* PNL-10821, Pacific Northwest National Laboratory, Richland, Washington.

Appendix A

Implications of Treating Bubble Gases as Volumeless Solutes

Appendix A

Implications of Treating Bubble Gases as Volumeless Solutes

In this study, the gas bubbles released during salt well pumping are modeled as air bubbles containing passive tracer gases. This assumption results in a significant simplification for modeling because solute gases do not affect the physical properties of the gas phase. For salt well pumping, the model is reasonably good, and we expect the qualitative results and conclusions in this report to be valid. The drawback to this approach is that when a water-soluble gas such as ammonia partitions into the gas phase, there is no resulting change in gas volume. Likewise, the solute gases exert no pressure inside the salt cake or in the dome space. Ultimately, we would like to modify STOMP to model concentrated solute gases that are miscible in air and with each other, but such code modification is beyond the scope of the present study.

In STOMP, the solute gases are governed by an equilibrium partition coefficient between the gas and liquid phases:

$$K_{eq} = \frac{c_{gas}}{c_{liq}}$$

where c_{gas} is the molar concentration of the solute in the gas phase (e.g., moles solute per volume gas phase) and c_{liq} is the molar concentration in the liquid phase (moles solute per volume liquid). Such a relationship is equivalent to a Henry's Law approach (as in Norton and Pederson 1994):

$$P_i = y_i P_{tot} = \frac{m_i}{K_H}$$

where P_i is the partial pressure of the solute in the gas phase, y_i is the solute mole fraction in the gas phase, P_{tot} is the total (absolute) ambient pressure, K_H is the Henry's Law constant for the solute, and m_i is the molality of the solute in the liquid phase (in moles of solute per mass of solvent). The K_{eq} used by STOMP can be related to the K_H used by Norton and Pederson:

$$K_{eq} = \frac{1}{RT\rho_{liq}K_H}$$

where R is the ideal gas constant, T is the absolute temperature, and ρ_{liq} is the solvent density.

The implication of a Henry's Law relationship between liquid and gas phase solute

concentrations is that changes in the ambient pressure can result in fluxes of solute between the liquid and gas phases. The presence of multiple gases of varying aqueous solubility moderates this effect somewhat. To illustrate this point, consider the effect on a submerged bubble when the ambient pressure decreases by half. According to the ideal gas law, the bubble volume increases by a factor of two. However, the reduction in pressure also affects the equilibrium between dissolved and vaporized solute according to Henry's Law. Since the partial pressure of the solute vapor has decreased by a factor of two, solute will be driven out of solution into the gas to reduce its liquid phase concentration and restore the equilibrium. Assuming a large liquid-phase concentration (so that x_i changes very little), the factor of two reduction in pressure would cause a factor of two increase in the mole fraction vapor, y_i. This volatilization would result in an increase in bubble volume beyond the factor of two predicted by the ideal gas law. Using the values in the 2-D modeling, the 15% soluble gas initial concentration would increase to 30%, resulting in a bubble volume increase of 21% (assuming no other gases volatilized).

Since solute gases are volumeless in STOMP, however, it neglects these volume changes. The model will therefore underpredict the gas saturation in elements with trapped gas in the presence of soluble gases. At the percolation threshold, gas release rates depend on the gas saturation. Thus gas release rates may be underpredicted by STOMP when the material is near the maximum trapped gas saturation. This effect includes the rate of release of insoluble gases such as hydrogen, since bubble expansion by soluble gas volatilization beyond the percolation threshold would liberate both types of gases. However, the total amount of insoluble gas released when the tank is completely drained is not affected, since essentially all of the insoluble gas is released in either case. Furthermore, the total soluble gas release will in practice be controlled by the ventilation rate in the dome space. From the results in this study, it appears that salt well pumping will make the salt cake an enhanced source of vapor, causing the dome space to remain saturated with soluble gas vapor.

For the 2-D modeling, the material is initially quite close to the percolation threshold. The average pressure change in the salt cake is a factor of 1.7. From these arguments, it appears that the model may be underpredicting the rate of insoluble gas release somewhat. However, since the additional volume created by such a pressure change is small (less than 20%), and since draining and release occur over periods of 60–200 days, it seems unlikely that the insoluble gas release rate is severely underpredicted. The total insoluble gas release prediction is unaffected. Finally, the soluble gas release rate would also increase slightly, but that increase is unlikely to affect the ultimate soluble gas content of the dome space.

Appendix B

Sample Input File for STOMP

Appendix B

Sample Input File for STOMP

This input file corresponds to Case Study 1.

```
~Simulation Title Card
1,
Simulation of SST Entrapped Gas Release During Salt Well Pumping,
LM Peurrung,
Pacific Northwest National Laboratory,
Tuesday, April 16, 1996,
10:00:00 AM,
5,
This simulation shows the release of trapped gas during salt-well
pumping.
Note that the tracer gas occupies no volume.
This file represents a 1-D wedge with 160 vertical nodes with hc
= 30 cm/hr.
This version: fill to the top, drain in 100 days.
Initial saturation is 0.05; maximum trapped air is 0.10.

~Solution Control Card
Normal,
Water-Air Transport,
1,
0,day,140,day,0.1,hr,0.25,day,1.25,16,1.E-6,
1,yr,1,yr,1300,
Variable,
Variable,
0,

~Grid Card
Uniform Cylindrical,
1,1,160,
1,ft,
30,deg,
0.125,ft,

~Rock/Soil Zonation Card
1,
Porous Sludge,1,1,1,1,1,160,

~Mechanical Properties Card
Porous Sludge,2650,kg/m^3,0.4,0.4,,,Constant,1.0,1.0,

~Hydraulic Properties Card
Porous Sludge,30.,hc:cm/hr,30.,hc:cm/hr,30.,hc:cm/hr,
```

```
~Saturation Function Card
Porous Sludge,van Genuchten
Entrapment,5.,1/m,10.,1/m,1.25,0.01,0.1,

~Aqueous Relative Permeability Card
Porous Sludge,Mualem,,

~Gas Relative Permeability Card
Porous Sludge,Mualem,,

~Solute/Fluid Interaction Card
1,
tracer,1.e-9,m^2/s,1.e-5,m^2/s,Constant,1.e+10,m^3/m^3,continuous
,1.e+10,d,
0,

~Solute/Porous Media Interaction Card
Porous Sludge,0,m,0,m,
tracer,0,m^3/kg,

~Initial Conditions Card
Aqueous Pressure,Gas Pressure,
5,
Trapped Air Saturation,0.05,,,,,,,,1,1,1,1,1,160,
Gas Pressure,101325.,Pa,,,,,-11.77,1/m,1,1,1,1,1,160,
#Aqueous Pressure,160653.1,Pa,,,,,-9793.51,1/m,1,1,1,1,1,160,
Aqueous Pressure,160500.,Pa,,,,,-9793.51,1/m,1,1,1,1,1,160,
Temperature,20.0,C,,,,,,,1,1,1,1,1,160,
Solute Gas Volumetric Conc.,tracer,1.,1/m^3,,,,,,,1,1,1,1,1,160,

~Boundary Conditions Card
2,
Top,Zero Flux,Dirichlet,Gas Conc.,
1,1,1,1,160,160,1,
0,day,,,101253.47,Pa,1.0,0.,1/m^3,
# Gas pressure here should be initial condition gas pressure at
the bottom
# minus an air head of (tank height - half a node width)
Bottom,Neumann,Zero Flux,Outflow,
1,1,1,1,1,1,3,
0,day,-0.35,mm/hr,,,1.0,,,
100,day,-0.35,mm/hr,,,1.0,,,
100,day,0.,mm/hr,,,1.0,,,

~Output Control Card
17,
1,1,1,
1,1,10,
1,1,20,
1,1,30,
1,1,40,
1,1,50,
1,1,60,
```

```
1,1,70,
1,1,80,
1,1,90,
1,1,100,
1,1,110,
1,1,120,
1,1,130,
1,1,140,
1,1,150,
1,1,160,
40,40,day,ft,5,5,5,
6,
Phase Condition,,
Trapped Air,,
Gas Saturation,,
Aqueous Pressure,Pa,
Gas Pressure,Pa,
Solute Gas Conc.,tracer,,
0,
#20.,day,
5,
Trapped Air,,
Gas Saturation,,
Aqueous Pressure,Pa,
Gas Pressure,Pa,
Solute Gas Conc.,tracer,,

~Surface Flux Card
3,
Gas Volumetric Flux,m^3/day,m^3,Top,1,1,1,1,160,160,
Solute Flux,tracer,sol/day,sol,Top,1,1,1,1,160,160,
Aqueous Volumetric Flux,m^3/day,m^3,Bottom,1,1,1,1,1,1,
```

Distribution

No. of Copies

Offsite

5 Los Alamos National Laboratory
P.O. Box 1663
Los Alamos, NM 87545
Attn: D. R. Bennett, K575
J. R. White, K575
K. Pasamehmetlogu, K575
J. Spore, K575
E. A. Rodriguez, K575

C. W. Forsberg
Oak Ridge National Laboratory
P.O. Box 2008 MS 6495
Oak Ridge, TN 37831

S. E. Slezak
Sandia National Laboratory
P.O. Box 5800 MS 1004
Albuquerque, NM 87110

B. C. Forsberg
P.O. Box 271
Lindsborg, KA 67456

Onsite

4 DOE Richland Operations Office

K. Chen	S7-54
C. A. Groendyke	S7-54
G. W. Rosenwald	S7-54
J. M. Gray	S7-54

1 Los Alamos Technical Associates

J. Siemer	S7-54

No. of Copies

17 Westinghouse Hanford Company

S. A. Barker	R2-11
W. B. Barton	R2-11
R. E. Bauer	S7-14
S. L. Engstrom	R2-50
K. M. Hodgson	R2-11
G. D. Johnson (3)	S7-15
N. W. Kirch	R2-11
M. A. Lane	S8-05
J. W. Lentsch	S7-15
W. H. Meader	S8-05
D. M. Ogden	H0-34
D. A. Reynolds	R2-11
G. R. Sawtelle	A3-37
E. R. Siciliano	H0-31
R. J. Van Vleet	R3-27

55 Pacific Northwest Laboratory

Z. I. Antoniak	K7-15
S. Q. Bennett	K7-90
M. E. Brewster	K9-62
J. L. Buelt	P7-41
J. W. Brothers (5)	K9-20
S. M. Caley	P7-41
P. A. Gauglitz (15)	P7-41
T. E. Michener	K7-15
B. J. Palmer	K7-15
L. R. Pederson	K2-44
L. M. Peurrung (15)	P7-41
S. D. Rassat	P7-41
A. Shekarriz	K7-15
C. S. Simmons	K9-33
C. W. Stewart	K7-15
M. D. White	K9-36
Information Release (7)	K1-06